ACOUSTIC PROPERTIES OF ANTIBUBBLES

Nicole Anderton

A dissertation submitted to the Faculty of Engineering and the Built Environment, University of the Witwatersrand, Johannesburg, in fulfilment of the requirements for the degree of Master of Science in Engineering.

Johannesburg, 26 June 2020

To Janet and Steve Smith, Keagan Bester and Rose Mbaso, your unwavering love and support throughout my tertiary studies has meant the world to me.

Declaration

I declare that this dissertation is my own, unaided work. It is being submitted for the Degree of Master of Science at the University of the Witwatersrand, Johannesburg. It has not been submitted before for any degree or examination at any other University.

_____

Nicole Anderton

Signed on the _____ day of _____ _____ at the University of Witwatersrand, Johannesburg

Abstract

Antibubbles are gas bubbles with incompressible liquid cores. When stabilised, antibubbles may have specific acoustic properties that allow for localised drug delivery. The aim of this research was to investigate these acoustic properties. Footage of three types of antibubble-containing media under the influence of ultrasound were analysed. Of the media, two contained antibubbles with different amounts of stabilising endoskeletal content, and the third contained reference bubbles which comprised of core-less antibubbles. Image segmentation and processing was used to analyse the footage and quantify the changes in individual antibubble and bubble size throughout sonication. Antibubble oscillation was found to be symmetric at a low acoustic amplitude of 200 kPa and highly asymmetric at a high, but still clinically safe, acoustic amplitude of 1 MPa. This was a result of the presence of their liquid droplet cores hampering negative excursion under high amplitude sonication. It was also found that under low amplitude sonication, micron-sized antibubbles oscillate more reliably and stably than their bubble counterparts. Additionally, it was observed that only a single pulse of high amplitude ultrasound was enough to cause an antibubble to rupture. This indicates that at lower acoustic amplitudes antibubbles can be carefully controlled and used in diagnostics, and at higher acoustic amplitudes they can be made to rupture and release their — therapeutic — contents.

Acknowledgements

I wish to thank Dr Albert T. Poortinga from the Eindhoven University of Technology for supplying the antibubble samples and Mr Ri-ichiro Shimizu, Mr Ryuosuke Matsumoto and Prof. Nobuki Kudo from the University of Hokkaido for supplying the high-speed video footage analysed in this thesis.

I'd also like to thank my supervisor Prof. Michiel Postema for affording me the opportunity to gain the experience, discipline and knowledge required to put this dissertation together.

Lastly, I would like to thank my colleagues, friends and family, with special mentions to Mr Keagan M. Bester and Mr Craig S. Carlson for their constant advice and readiness to find and correct my seemingly abundant supply of misspellings.

Contents

List of Figures

List of Tables

Nomenclature

Abbreviations

AB1	antibubble type 1	-
AB2	antibubble type 2	-
P2P	Peak to Peak Pressure	Pa
PNP	Peak Negative Pressure	Pa
PPP	Peak Positive Pressure	Pa
PRT	Pulse Repetition Period	s
REF	reference bubble	-

Symbols

f_c	centre frequency	Hz
f_d	damped response frequency	Hz
p_v	vapour pressure	Pa
p_0	ambient pressure	Pa
p_cr	critical pressure	Pa
u	approach velocity	$\mathrm{m{\cdot}s^{-1}}$
A	cross-sectional bubble area	$\mathrm{m^2}$
$E_{\mathrm{f},i}$	total free surface energy	N·m
E_k	kinetic energy	J
E_s	surface energy	N·m
MI	Mechanical Index	-
N	number of fragments	-
N_at	number of pixels with greyscale value above the threshold value	-
N_bt	number of pixels with greyscale value below the threshold value	-

N_{tot}	total number of pixels	-
P(t)	ultrasound pressure	Pa
R	instantaneous radius	m
R_{cr}	critical radius	m
R_{d}	antibubble internal liquid droplet core radius	m
R_{m}	mean radius	m
R_{fin}	final radius	m
R_{min}	minimum radius	m
R_{max}	maximum radius	m
R_0	equilibrium radius	m
$\dot{R}$	instantaneous velocity of expansion/contraction	$\text{m}\cdot\text{s}^{-1}$
$\ddot{R}$	instantaneous acceleration of expansion/contraction	$\text{m}\cdot\text{s}^{-2}$
T	Period	s
We	Weber number	-
η	bulk fluid viscosity	Pa·s
γ	polytropic exponent of the gas	-
ρ	liquid density	$\text{Kg}\cdot\text{m}^3$
σ	surface tension	$\text{N}\cdot\text{m}^{-1}$
σ_{at}	greyscale variance above threshold value	-
σ_{bt}	greyscale variance below threshold value	-
σ_{icv}	in-class variance	-
ξ^+	positive excursion	m
ξ^-	negative excursion	m

Chapter 1

Introduction

The use of ultrasound to safely manipulate targeted drug delivery agents containing chemotherapeutics has the potential to greatly reduce the tissue damage caused by the current systematic drug delivery methods in use [1]. Ultrasonic drug delivery agents that are capable of safely and reliably transporting, and then releasing chemotherapeutics at a target site have not yet been identified. Antibubbles have been suggested as a potentially viable option, although their acoustic properties are not yet fully understood [2]. This dissertation details an investigation into the properties of antibubbles that may make them suitable carriers of chemotherapeutics for the purpose of ultrasound targeted drug delivery.

1.1 Problem statement

Currently, there is no way to safely transport highly toxic chemicals such as chemotherapeutics through the body and then release them at a target site. This leaves patients undergoing chemotherapeutic treatment to suffer the harsh systematic side effects of these drugs. The ability to use acoustically active microparticles as chemotherapeutic agents would allow for the use of ultrasonic drug delivery, a non-invasive, inexpensive and reliable method of drug delivery. While attempts to use ultrasound contrast agent microbubbles as chemotherapeutic drug carriers have not met with success, antibubbles have been suggested as a potential alternative owing to their incompressible liquid droplet cores. Further investigation into the acoustic properties of antibubbles is required before they can be considered viable for use in targeted chemotherapeutic drug delivery.

1.2 Research question

At a low ultrasonic amplitude, do antibubbles oscillate less linearly than microbubbles, and can they be made to rupture at a higher, but still medically safe, ultrasonic amplitudes?

1.3 Objectives

1. To investigate the expansion-only hypothesis of antibubbles. This hypothesis was coined in [39] and refers to the theory that antibubbles will not contract beyond the size of their internal droplet cores and will thus experience greater spherical oscillation asymmetry than microbubbles whilst under sonication.

2. To determine whether antibubbles oscillate in a more reliable and stable manner than microbubbles when exposed to the same, low amplitude, ultrasonic conditions. Where reliability is defined as the similarity of oscillation of antibubbles of the same type under the same acoustic conditions, and stability is defined as the similarity of oscillation for the same antibubbles under repeated exposure to the same acoustic conditions.

3. To determine whether antibubbles undergo fragmentation under the same high amplitude, but still clinically safe, ultrasound conditions that microbubbles do.

1.4 Organisation of research

The first chapter consists of a short introduction, followed by the problem statement, research questions and objectives. This focuses the reader on the intentions of the research and provides context for the detail that follows. The background to the problem, with relevant literature, is explored in chapter two. The necessary theory required to investigate the acoustic properties of antibubbles is provided in chapter three; medical ultrasound and the acoustic properties of both microbubbles and antibubbles are discussed. Chapter four details the sample preparation techniques, experimental setup and procedure, image processing implemented and the analysis thereof. The results are presented in chapter five. A distribution of data is presented, followed by the results per each objective. Chapter six details a discussion of the results observed in the previous chapter and chapter seven concludes the investigation.

Chapter 2

Background

The field of medical ultrasonics is rapidly expanding, with ultrasonic imaging becoming the most commonly used imaging modality in clinical settings [3]. It's popularity can be attributed to the fact that this diagnostic technique is a safe, reliable and comparatively cheap when compared to other imaging modalities currently in use [4]. In recent years ultrasound contrast agents which are effectively encapsulated, artificial, gas-filled microbubbles of less than 10 μm in size, have been instrumental in expanding the imaging potential within the field [5, 6, 7]. These microbubbles are currently used in ultrasonic imaging to differentiate blood from the otherwise acoustically indistinguishable surrounding tissue [8, 9]. The characteristic acoustic properties of microbubbles allows them to oscillate when exposed to low amplitude ultrasound, making them ideal markers for blood when looking for perforated or damaged tissue [10].

The ability to use ultrasound to manipulate microbubbles has inspired researchers to investigate the therapeutic potential of ultrasound contrast agents for applications such as targeted drug delivery. Further fuelling the interest in ultrasound-assisted drug delivery is a phenomena known as sonoporation. Sonoporation is the transient permeation and resealing of cell membranes that occurs during ultrasound exposure. Ultrasound-aided drug delivery and in-gene delivery are applications that stand to benefit greatly from the introduction of controlled sonoporation, as it could be utilised in trans-membrane delivery and as a method to increase cellular uptake of macromolecules [11, 12, 13]. The use of sonoporation for the increased uptake of chemotherapeutics during cancer treatment has proven to be a promising one [14, 15]. Sonoporation alone will not stop the damage inflicted on the rest of the body, as the current systematic drug administration causes damage to the entire body. The addition of targeted drug delivery and release would greatly reduce the current systematic damaged caused [1].

Microbubbles have been considered as a delivery tool for chemotherapeutics, however, attempts to add chemotherapeutics to microbubbles have met with little success [3]. The commonly attempted method has been to incorporate the load into the shell of a microbubble [16, 17]. The addition of the drug layer makes the microbubble less oscillatory, ultimately stunting it's ability to rupture at clinically safe amplitudes. If the microbubbles cannot consistently be made to rupture, drug delivery cannot

be guaranteed. There is also the problem of quantity, only a minute amount of the drugs could be stored within the shell of a microbubble.

If the chemotherapeutics could be inserted into the gas core of a stabilised bubble, an antibubble would result. Not only would this greatly increase the potential load volume, but it could also allow for both better stability at lower amplitudes and consistency of rupture at higher clinically safe amplitudes [1]. Antibubbles are effectively liquid droplet cores, surrounded by a layer of gas. This phenomena sounds far fetched, but actually occurs regularly in nature when a liquid jet is turbulently introduced into a pool of the same substance and a layer of air becomes trapped between the two liquid surfaces and remains trapped there as the jet tapers off [18]. Despite their abundance, they will only form under very specific conditions which are limited by the following factors; the initial velocity, radius and height above the liquid pool of the liquid column as well as the surface tension of the liquid [19].

Whilst the liquid cores of antibubbles are assumed incompressible, the compressibility of the surrounding gas layer determines how quickly it drains away [19]. Without intervention, antibubbles can only maintain their stability for a limited period of time, with a maximum lifespan recorded as just shy of 1000 seconds [20, 21]. The size of an antibubble largely determines its life expectancy, as those with diameters in the micrometer range have been shown to last no longer than a single second [8, 22]. Both the liquid droplet core and surrounding gaseous layer can however be stabilised through the addition of encapsulating shells. The electrostatic forces exerted by these shells hinder the inner liquid droplet core from coalescing with the outer surrounding liquid, drastically extending the lifespan of the antibubble [2, 23]. The ability to stabilise these small particles has made them a promising alternative to the microbubbles currently used in ultrasonic drug delivery applications as their load volumes are much higher [8, 23].

In contrast to the unhindered oscillation of microbubbles at low amplitudes, the incompressible nature of the liquid core of antibubbles implies that they should oscillate asymmetrically under similar conditions [2]. A simulation study indicated that when antibubbles and bubbles of the same size were exposed to the same ultrasonic pulses, the antibubbles expanded more than the microbubbles, and contracted less [24]. If this finding holds in reality, antibubbles should be more reliable and stable than microbubbles, as rupture occurs as a result of rapid, uncontrolled contraction [1, 8]. Their stable oscillation at low ultrasonic amplitudes, combined with their ability to rupture at higher, but still clinically safe, amplitudes could mean that drugs stored within the liquid core of antibubbles can be safely manipulated through the blood stream and then released at a targeted site when required [1].

Chapter 3

Theory

Before the acoustic properties of antibubbles and microbubbles can be understood, an understanding of the principles of ultrasound and it's application in medicine is imperative in determining the effects on bubbles and antibubbles. This chapter details the necessary ultrasound physics as well as the effect that ultrasound will have on antibubbles and microbubbles owing to their acoustic properties.

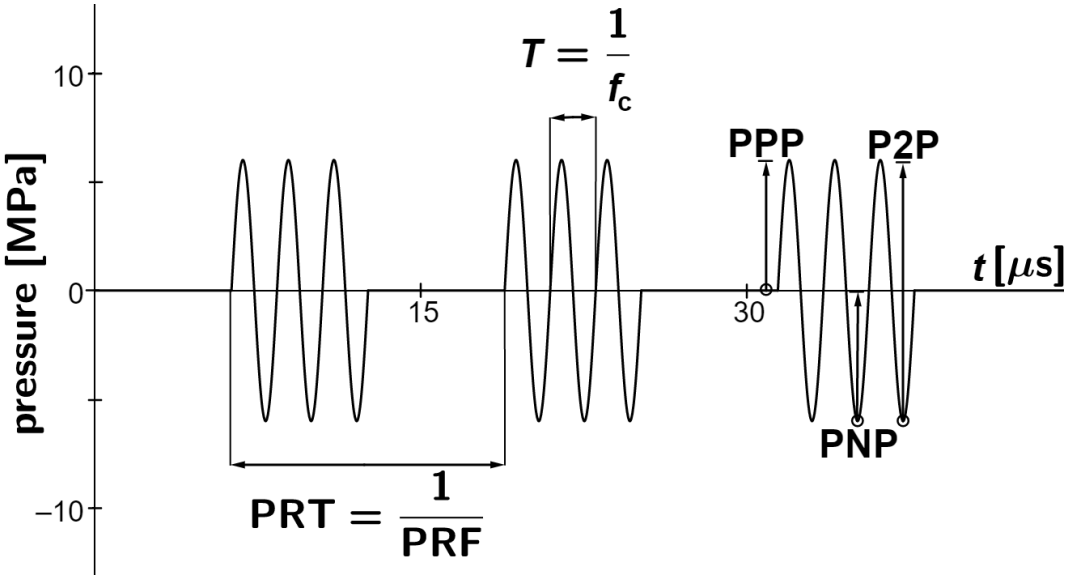

Figure 3.1: Visual representation of an ultrasound pulse sequence with each pulse consisting of three cycles at centre frequency (f_C). The dominant period (T), peak-positive pressure (PPP), peak-negative pressure (PNP), peak-to-peak pressure (P2P), pulse-repetition period (PRT), and pulse-repetition frequency (PRF) are clearly shown. Reprinted from [4].

Ultrasound waves are vibrations that propagate through matter at frequencies above 20 kHz. An ultrasound field at a given location can be characterised according to it's centre frequency, dominant period, pulse length, duty cycle, peak-negative and positive pressures, peak-to-peak pressure, pulse-repetition time and pulse-repetition frequency [25]. The centre frequency is the number of sonic cycles per second, with the dominant period being it's reciprocal. Pulse length is the total duration of a pulse. Duty cycle, given as a percentage, is the transmission time per each pulse. The pulse-repetition period is the time lapsed between the beginning of one pulse

and the beginning of the next pulse. Pulse-repetition frequency is the reciprocal of the pulse-repetition period [25, 26]. Figure 3.1 provides a visual representation of the described characteristics.

Safe use of ultrasound in medicine is of the highest importance, and is thus covered here. When the peak-negative acoustic amplitude of ultrasound surpasses the cavitation threshold, cavitation occurs. This is observed by the formation of bubbles in a liquid [26, 27, 28, 29]. This phenomenon has applications in drug delivery, but has also been observed to be the cause of harmful bio-effects [30, 31, 32]. The mechanical index (MI) gives an indication of the potential mechanical damage caused by inertial cavitation and is used to estimate the relative safety of ultrasound medical equipment.

The mechanical index is born out the relationship between the threshold peak negative pressure ($\mathrm{PNP_{TH}}$), at which cavitation takes place, and the frequency of the applied ultrasound. This relationship is: $\mathrm{PNP_{TH}^{2.10}} \propto f$" in water [33]. The MI of an ultrasound pulse is calculated as follows [26]:

$$\mathrm{MI} = \frac{\mathrm{PNP}}{\sqrt{f_\mathrm{c}}} \tag{3.1}$$

where PNP, given in MPa and normalised by 1 MPa, is the maximum peak negative pressure within the sound field and f_c is the centre frequency of the ultrasound signal, given in MHz and normalised by 1 MHz [26].

The mechanical index is born out the relationship between the threshold peak negative pressure ($\mathrm{PNP_{TH}}$), at which cavitation takes place, and the frequency of the applied ultrasound. This relationship is described by $\mathrm{PNP_{TH}^{2.10}} \propto f$ in water [33].

A mechanical index of less than 0.3 is recommended for medical diagnostic applications [26]. The use of ultrasound with mechanical index values of between 0.3 and 0.7 has been shown to cause minor damage to soft tissues such as human intestines. Mechanical index values that are greater than 0.7 are considered unsafe for diagnostic applications as this MI value is considered the threshold after which the risk of cavitation is significant [3]. The absolute MI limit for commercial medical imaging scanners is set at 1.9 [34].

Ultrasonic medical devices make use of multi-element transducers to generate ultrasonic fields [26]. Ultrasound frequencies above 500 kHz are generally used for cell or particle manipulation, whilst the non-destructive evaluation of cellular structure, such as that used in biomicroscopy, is often carried out using ultrasound with frequencies in the range of 10–100 MHz [35, 36].

3.1 Bubble and antibubble dynamics

Antibubbles are often described as the inverse of bubbles, this inverse relationship can readily be observed in Figure 3.2 [18, 37, 38, 39]. In this instance the antibubble is surrounded by the same substance from which its core is formed and the bubble is surrounded by the same gas that resides within it's liquid outer surface. When these particles are strengthened with stabilising shells and exist within the same medium however, the only differentiating factor between the two particles would be the liquid core inside of the antibubble. The structural and acoustic properties of stabilised microbubbles, along with the effect that the addition of a stabilised liquid droplet core has on them, is discussed in this section.

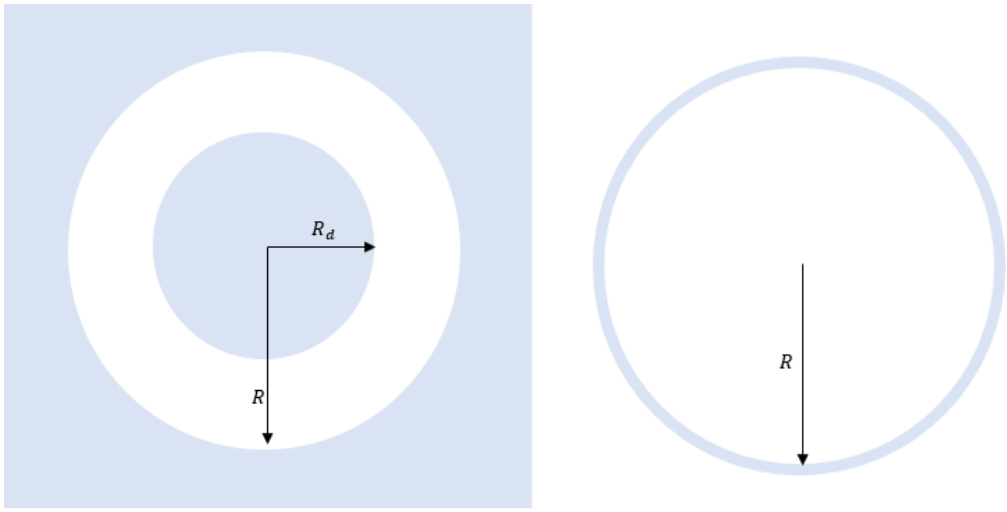

(a) Antibubble (b) Bubble

Figure 3.2: Side by side schematics of an (a) antibubble and (b) a bubble from which the inverse nature of the two is clearly observed. The white areas represent gas whilst the blue areas represent liquid.

When subjected to an acoustic field, a number of forces act on an (anti)bubble. The (anti)bubble will oscillate in response to these forces, generating a spherical wave which radiates outwards omnidirectionally [40]. The (anti)bubble may also translocate and, if in the presence of other (anti)bubbles, attract or repel them [41]. All of these movements are dependent on the resonance frequency of the (anti)bubble, which in turn is dependant on it's mechanical properties.

In the equations to follow, the liquid surrounding antibubbles and bubbles is assumed incompressible and viscous and the gas within antibubbles and bubbles is assumed

to be polytropic. The outer shells of both antibubbles and bubbles are also assumed to have negligible thickness.

3.1.1 Oscillation

Antibubbles and bubbles will undergo alternate positive excursion and negative excursion when exposed to the respective negative and positive cycles of a periodic acoustic signal. At low acoustic amplitudes bubbles oscillate in a spherical manner and at high acoustic amplitudes they oscillate in a non-linear manner which can lead to rupture. At low amplitudes antibubbles are expected to oscillate in a more asymmetric, but still spherical manner as the incompressible liquid droplet core should hamper it's negative excursion. Additionally the larger the droplet core, the more pressure inside of the antibubble, resulting in theoretically greater positive excursion than that which would be experienced by bubbles of the same size. The droplet core itself is not expected to oscillate during sonication owing to it's incompressibility [42].

The higher internal pressure in antibubbles an be explained by [42]:

$$p_g = p_0 \left(\frac{R_0 - R_\mathrm{d}}{R - R_\mathrm{d}}\right)^\gamma, \tag{3.2}$$

where p_g is the instantiation gas pressure, p_0 is the ambient gas pressure, γ is the polytropic exponent of the gas, R_0 is the equilibrium radius of the antibubble, R is the instantaneous radius of the antibubble and R_d is the radius of the internal liquid droplet core of the antibubble. For core-less bubbles R_d will be equal to zero.

The Rayleigh-Plesset equation is considered the fundamental equation of bubble dynamics as it describes the non-linear behaviour of bubble dynamics. This equation, which has been adapted from [43] to include the liquid droplet core of an antibubble is [42]:

$$R\ddot{R} + \tfrac{2}{3}\dot{R}^2 = \tfrac{1}{\rho}\left[\left(p_0 - p_\mathrm{v} + \tfrac{2\sigma}{R_0}\right)\left(\frac{R_0^3 - R_\mathrm{d}^3}{R^3 - R_\mathrm{d}^3}\right)^\gamma + p_\mathrm{v} - \tfrac{2\sigma}{R} - \tfrac{4\eta\dot{R}}{R} - p_\mathrm{v} - P(t)\right]. \tag{3.3}$$

Here $\dot{R}$ and $\ddot{R}$ are the instantaneous velocity and corresponding acceleration of positive or negative excursion of the antibubble. $P(t)$ is the ultrasound pressure, ρ is the liquid density, p_v is the vapour pressure, η is the viscosity of the surrounding

fluid and σ is the surface tension. It is clear from (3.3) that increasing the driving amplitude of applied ultrasound results in more asymmetric radial excursion [42].

At low mechanical index values (MI < 0.1) the positive an negative excursion is equal and symmetrical, allowing the linearisation of (3.3) [26]. Under these conditions (anti)bubbles behave like a mass-spring-dashpot systems. This results in the following equation for the damped resonance frequency of an antibubble [1]:

$$f_{\mathrm{d}} = \left(\frac{1}{2\pi R_0\sqrt{\rho}}\right)\sqrt{3\gamma\frac{\left(p_0 - p_{\mathrm{v}} + \frac{2\sigma}{R_0}\right)}{1-\left(\frac{R_{\mathrm{d}}}{R_0}\right)^3} + \frac{2\sigma}{R_0} - \frac{4\eta^2}{\rho R_0^2}}. \tag{3.4}$$

From this equation it can be observed that the non-zero internal liquid droplet radius of an antibubble should result in a higher resonance frequency than that of a similarly sized bubble [1, 26]. It can also be observed that antibubbles that have inner droplet cores with very small radii compared to their outer radius ($\frac{R_{\mathrm{d}}}{R_0} \to 0$) will behave like bubbles, for which R_{d} is always equal to zero. When the radius of the internal droplet core is comparitivly large ($\frac{R_{\mathrm{d}}}{R_0} \to 1$) however, antibubbles are no longer expected to behave like bubbles when exposed to the same conditions [42].

3.1.2 Fragmentation

When exposed to ultrasound with a high mechanical index value (MI > 0.6) a violent collapse follows the positive excursion phase of bubble oscillation. Fragmentation (the dominant distribution mechanism for microbubbles with an elastic shell) occurs during this collapse if the kinetic energy exceeds the surface energy of the bubble and the surface instabilities are big enough [9, 44]. Fragmentation has been associated with inertial cavitation at high MI values.

If the (anti)bubble has a monolayer shell of negligible thickness, the kinetic energy (E_{k}) of the bubble can be approximated by [26]:

$$E_{\mathrm{k}} \approx 2\pi\rho R^3\dot{R}^2. \tag{3.5}$$

The surface energy (E_{s}) of a bubble is given by [26]:

$$E_{\mathrm{s}} \approx 4\pi\rho R^2\sigma. \tag{3.6}$$

After fragmentation, the resulting bubble fragments contain more surface energy than the single bubble did prior to sonication [26]:

$$\textstyle\sum_{i=1}^{N} E_{\mathrm{f},i} = N^{\frac{1}{3}} E_{\mathrm{s}}, \tag{3.7}$$

where $E_{\mathrm{f},i}$ is the total free surface energy, N is the number of fragments into which the bubble breaks, which is related to the dominant spherical harmonic oscillation mode by the equation $N \approx n^3$. For the size range of the bubbles and antibubbles discussed in this study, more complicated oscillation and fragmentation models with modes larger than 2 can be ignored. Mode 2 oscillations have been observed for lipid-encapsulated microbubbles during which fragmentation into the expected 8 microbubbles was observed [26].

When the frequency of sonication is lower than the resonance frequency of the bubble, the liquid pressure change is slow and uniform compared to the natural time scale of the bubble. If the pressure is lowered to the point of being equal to the critical pressure (p_{cr}), a critical radius [26]:

$$R_{\mathrm{cr}} = \left[\frac{3\gamma}{2\sigma}\left(p_0 - p_{\mathrm{v}} + \frac{2\sigma}{R_0}\right)R_0^{3\gamma}\right]^{\frac{1}{3\gamma-1}}, \tag{3.8}$$

is reached and at this point cavitation occurs. This critical radius, also known as Blake's radius can be approximated by [26]:

$$R_{\mathrm{cr}} \approx 2R_0, \tag{3.9}$$

if the radius of the bubble is much smaller than double the surface tension divided by ambient pressure and if vapour pressure can be neglected [26].

3.1.3 Radiation forces

Primary radiation forces

The pressure gradient across the surface of a bubble or an antibubble in a sound field produces a primary radiation force. This force causes the translation of the particles in the direction of the sound field of a travelling wave and dictates the location of the particle in an acoustic standing wave [9]. The force acting on a particle is averaged for use in calculations, owing to the continuously varying pressure gradient in an acoustic field [9, 26].

When subjected to a standing wave, bubbles will move to a location which corresponds to the nodes or anti nodes of the pressure wave, depending on the angular frequency of the transmitted wave and the resonance frequency of the bubble. When the resonance frequency of a bubble is higher than the angular frequency of the transmitted wave, the bubble will move to the anti-node of the pressure wave. When the resonance frequency of a bubble is lower than the angular frequency of the transmitted wave,

the bubble will move to a node of the pressure wave. When the resonance frequency of a bubble and the angular frequency of the transmitted wave are equal, the bubble will stay in it's original location as the primary radiation force is equal to zero [40].

Secondary radiation forces

Oscillating bubbles and antibubbles under sonication produce secondary radiation forces owing to the presence of bubbles surrounding them. Bubbles that oscillate in phase with the sound field will move toward one another and aggregate. In contrast, bubbles that oscillate out of phase will repel one another [9, 41, 45].

3.1.4 Coalescence

Coalescence during ultrasound exposure can result when bubbles experiencing secondary radiation forces and collide with one another or when bubbles are close together and press upon one another during positive excursion. The mean resulting bubble radius (R_m) after two bubbles (with radii R_1 and R_2) have coalesced can be calculated as follows [26]:

$$\frac{2}{R_\mathrm{m}} = \frac{1}{R_1} + \frac{1}{R_2}. \tag{3.10}$$

The Weber number (We) of the colliding bubbles determines whether and how the bubbles will coalesce. This number can be determined by multiplying the square of the relative approach velocity (u) of the bubbles, the density of the surrounding fluid (ρ) and the mean radius of the bubbles, and dividing the result by the surface tension of the bubbles [26]:

$$\mathrm{We} = \frac{\rho u^2 R_\mathrm{m}}{\sigma}. \tag{3.11}$$

If the Weber number is less than 0.5 [46], bubbles will simply coalesce . If the Weber number is higher than this value, coalescence is preceded by surface flattening and will only take place if the liquid trapped between the two surfaces drains and reaches a critical thickness. When this critical thickness is reached, instability owing to the amplification of surface perturbations results in rupture during separation and the subsequent coalescence of the bubbles. The critical thickness is dependent on the thickness and surfactant concentration of the film between the two bubbles. For microbubble contrast agents of less than 10 μm in size, the critical thickness is assumed to be around 10 nm, as Van der Waals forces would become strong enough to ensure rapid rupture and subsequent coalescence at smaller film thickness values [26].

Chapter 4

Materials and methods

The acoustic properties of antibubbles were investigated through the analysis of experimental footage of antibubbles under sonication, as presented in [47]. In these experiments, antibubbles with varying amounts of endoskeletal content were exposed to a single pulse of ultrasound consisting of 3 cycles at a frequency of 1 MHz. Image processing techniques were used to identify and quantify changes in individual antibubble radius sizes throughout sonication. Analysis and comparison then followed. This chapter details the composition of the (anti)bubble samples used in the experiments, the experimental setup and procedure followed and the image processing techniques applied. The final section of this chapter makes use of the radius(time) curve generated from one of the antibubble experiments to indicate the points of interest examined in the results section that follows.

4.1 Sample preparation

For this study three antibubble types with differing cores were analysed under sonication. Two of the antibubble types contained liquid cores with varying amounts of endoskeletal content, and the third contained no core and therefore no endoskeletal content. The first type of antibubble, hereafter referred to as AB1, contained liquid cores of 2 vol% endoskeletal content. The second type of antibubble, hereafter referred to as AB2, contained liquid cores of 10 vol% endoskeletal content [47]. The third (anti)bubble, hereafter referred to as REF, functioned as the reference and contained no liquid cores, effectively making this type of antibubble a stabilised bubble [2]. A schematic representation of the structure of antibubble types AB1 and AB2 is compared to that of REF in Figure 4.1.

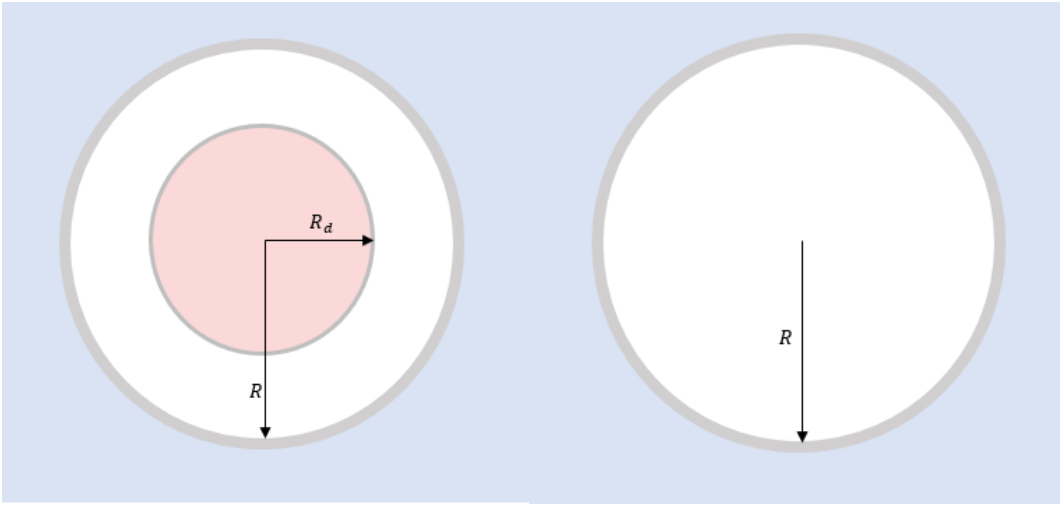

(a) Antibubble with endoskeletal content (b) Reference (anti)bubble

Figure 4.1: Side by side schematics of (a) the antibubble structure representing both AB1 and AB2, and (b) the bubble structure of REF. The light grey rings represent the thin stabilised shell within which the gas layer (white) and liquid droplet core (red) are contained and the blue represents the surrounding solution. The stabilised shells surrounding the antibubbles and cores have been assumed negligible in width.

A water-in-oil-in-water double emulsification process, was followed to create the stabilised antibubbles. The water contained 25% carbohydrate maltodextrin to counter the volatility of the hexane oil used. The varying quantities of endoskeletal content added to the liquid cores of the antibubbles was made of hydrophobically modified Zano 10 Plus zinc oxide nanoparticles (Umicore, Brussels), each of which being only around 30 nm in diameter. All of the outer antibubble shells were stabilised through the addition of Aerosil® R972 hydrophobised fumed silica particles (Evonik Industries AG, Essen, Germany). The silica particles were dispersed within the emulsion using an ultrasound probe, as the averaged size of a dispersed silica particle is well below 1 μm. The emulsions were frozen and freeze dried to remove the water and hexane used in the creation of the antibubbles [38].

A scanning electron microscope micrograph of an antibubble is shown in Figure 4.2, within which the skeletal structure can be seen beneath the ruptured silica membrane.

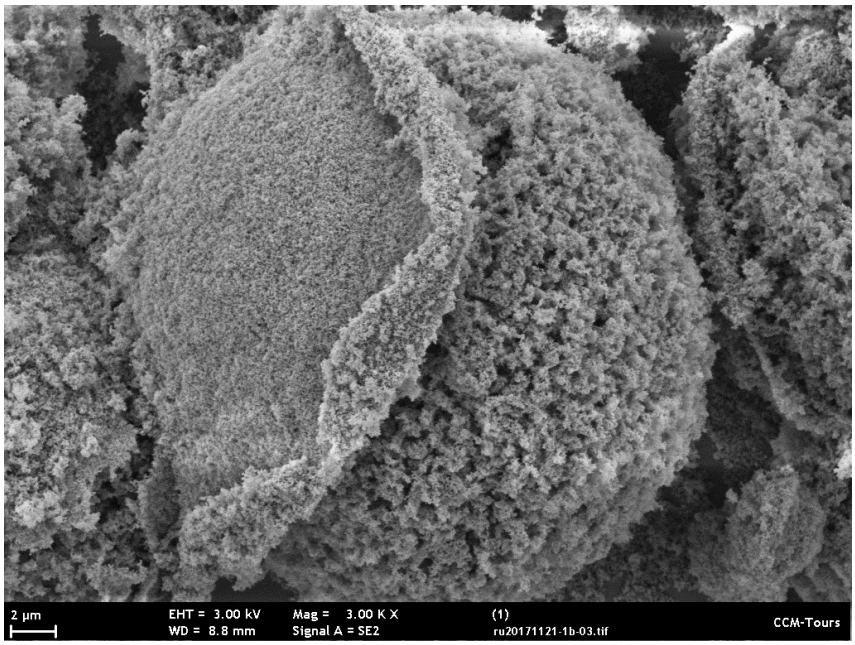

Figure 4.2: Scanning electron microscope micrograph of an AB1 antibubble. The thin outer silca membrane depicted in the figure has shrunk and ruptured as a result of the freeze drying process required for scanning electron microscopy. This allows for the visualization of the zinc oxide layer which forms the skeletal structure around the droplet core. The liquid core itself is not visible as all liquid components were evaporated during the freeze drying process. Reprinted from [39].

To make up the experimental samples of each type, 5 mg of freeze-dried (anti)bubbles were combined with 5 mL of 049-16797 distilled water (FUJIFILM Wako Pure Chemical Corporation, Chuo-Ku, Osaka, Japan). Each sample was mixed in a 15 mg FALCON® high quality polypropylene conical tube by gently shaking the container for one minute. Following this, 200 μL of the sample was then pipetted into the observation chamber, where the experiments and observation thereof took place.

4.2 Experimental setup

A specialised experimental setup was required for this investigation into the acoustic properties of antibubbles. The setup had to allow for the generation of a sound field, capable of targeting a 200 μL antibubble solution sample immersed in water. The investigation additionally required that the setup allow for clear observation and recording of the antibubbles within the sample, whilst under sonication.

To address the generation of a sound field an arbitrary AFG320 signal generator (Sony-Tektronicx, Shinagawa, Tokyo, Japan) and a UOD-WB-1000 wide-band power amplifier (TOKIN Coporation, Shiroishi, Miyagi, Japan) were connected to a laboratory assembled single element transducer. The transducer, with a centre frequency of 1 MHz had an aperture of 50 mm and a radius of 70 mm and was used to produce the 1 MHz ultrasound pulse consisting of three cycles for each experiment. As ultrasound travels poorly though air, a water tank into which the ultrasound transducer could be immersed was required.

A frequency of 1 MHz was chosen with tissue attenuation in mind. As the frequency of the applied ultrasound is increased, an almost linear increase in attenuation is observed, greatly reducing the penetration depth of the ultrasound [48, 49, 50].

A signal amplitude of 1 V, corresponding to an acoustic amplitude of 200 kPa PNP, was used to observe the stability of oscillation at low amplitudes and an amplitude of 5 V, corresponding to an acoustic amplitude of 1 MPa PNP, was used to observe whether fragmentation would occur at a higher amplitude. The 1 V pulse has a diagnostically safe MI of 0.2, whilst the 5 V pulse has a high MI value of 1. This MI value is above the threshold of cavitation, but a single pulse at this amplitude would not be expected to cause significant damage, as it is still far below the commercial medical imaging limit of 1.9. High intensity ultrasound has also been found to be a safe modality for palliative pancreatic pain relief [51, 52].

To address the observation of the samples while under sonication, an observation chamber was created by drilling a 10 mm diameter hole through the bottom of the water tank. A simple cover slip was placed over the bottom side of the hole, with another placed over the upper side of the hole. The water tank was placed onto the observation table of the IX70 inverted microscope (Olympus Corporation, Shinjuku-ku, Tokyo, Japan), leaving the LUMPlan FI/IR 40x (N.A. 0.8) objective lens fitted to the microscope to have full view of the observation chamber. The observation chamber was illuminated with a halogen lamp. A HPV-X2 high-speed camera (Shimadzu, Nakagyo-ku, Kyoto, Japan), with shutter speed set to 10 million frames per second, was attached to the microscope to record the experiments, with a total horizontal field of view of 145 μm [53]. A schematic overview of the setup used is depicted in Figure 4.3, and an illustration of the observation chamber within the setup is given in Figure 4.4.

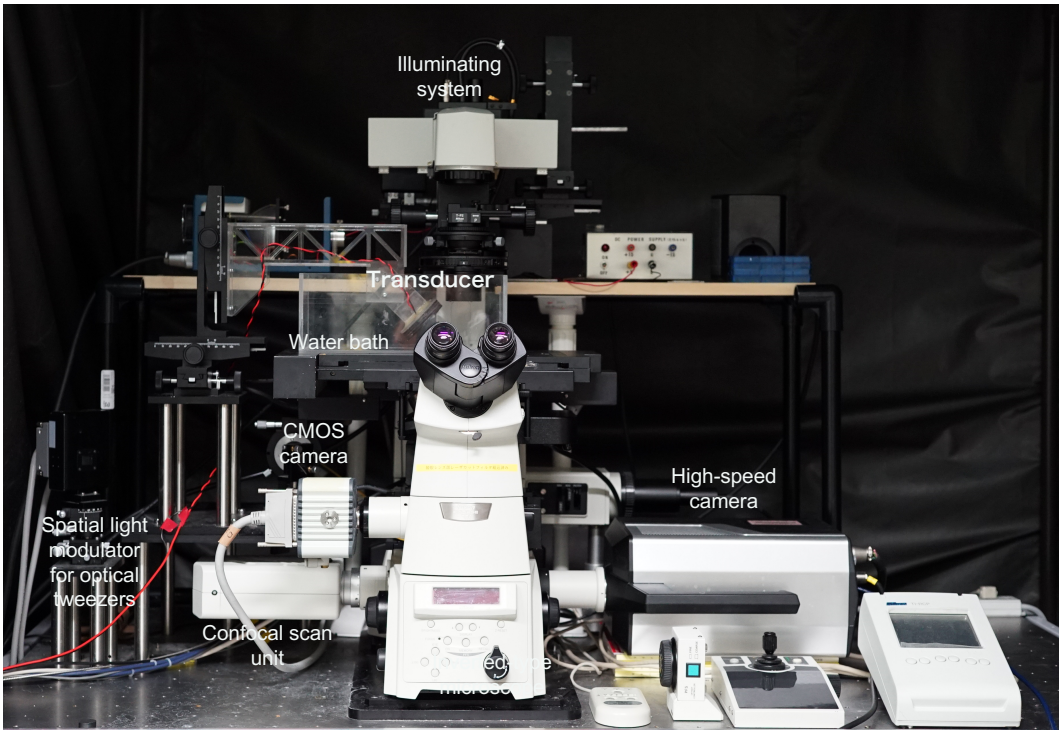

Figure 4.3: Experimental setup. Reprinted from [53].

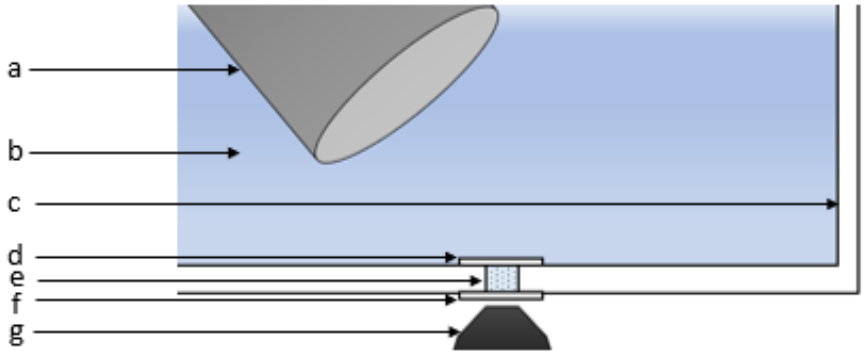

Figure 4.4: Illustration of a segment of the water bath showing the observation chamber cut-out. In this figure the transducer (a) is submerged in the degassed water (b) which is contained in the perspex water bath (c). The top cover slip (d) can be seen fixed above the observation chamber (e). The bottom cover slip (f) is fixed below the observation chamber, just above the objective lens (g).

4.2.1 Experimental procedure

Before the observation of samples under sonication could begin, the experiment components were carefully set up as described above. The water bath was emptied and turned upside down so that the bottom cover slip of the observation chamber could be removed. The sample was then prepared and pipetted into the observation chamber, with the cover slip replaced. Following this the water bath was turned upright, filled with de-gassed water and placed back onto the microscope. The power amplifier and signal generator were set to the desired output values, with the output of each switched off prior to testing.

The high-speed camera was then set to record and the signal generator and power amplifier was switched on to excite the ultrasound transducer. Following a single pulse of ultrasound, the power amplifier, signal generator and high speed camera were switched off, with each ultrasound pulse lasting 3 μs and each experimental recording lasting a total of 25.6 μs. The captured footage for the experiment was then downloaded and named according to the antibubble observed, time of experiment, amplitude of ultrasound applied and number of times the experiment had been repeated on that sample. In some instances the experiment was repeated on the same sample a further two times so as to later explore the effect of multiple pulses on each (anti)bubble type. After each experiment, or sets of experiments, the water bath was turned upside down so that the observation chamber could be emptied.

4.3 Image processing

Pre-recoded grey-scale videos were used for the observation and quantification of antibubble radius changes during sonication. A partially-automated method of extracting the necessary antibubble metrics from each frame of each experiment's footage was created using MATLAB® (The MathWorks, In., Natick, MA, USA). The steps that were followed to determine radius change over time for every antibubble during each experiment were repeated for each video.

The first step involved the manual identification and naming of each antibubble that could be accurately measured throughout the first 40 frames (4 μs) of the 256 frame (25.6 μs) video. The ultrasound pulse and thus the corresponding significant points of interest could be observed within the first 40 frames of each experiment's video and for this reason any antibubble that could not be accurately measured at

any point within the first 40 frames was excluded from the image processing analysis.

The pixel coordinates around each of the selected antibubbles in the first frame of the video were then noted so as to create a cropped image containing the antibubble of interest. As indicated by Figure 4.5, extra pixels surrounding the antibubble were included to allow for antibubble positive excursion, and potential translocation during the sonication process. The actual size of the antibubble could later be calculated, knowing that the 400 pixels constituting the X-axis of the image, equated to 145 μm in reality.

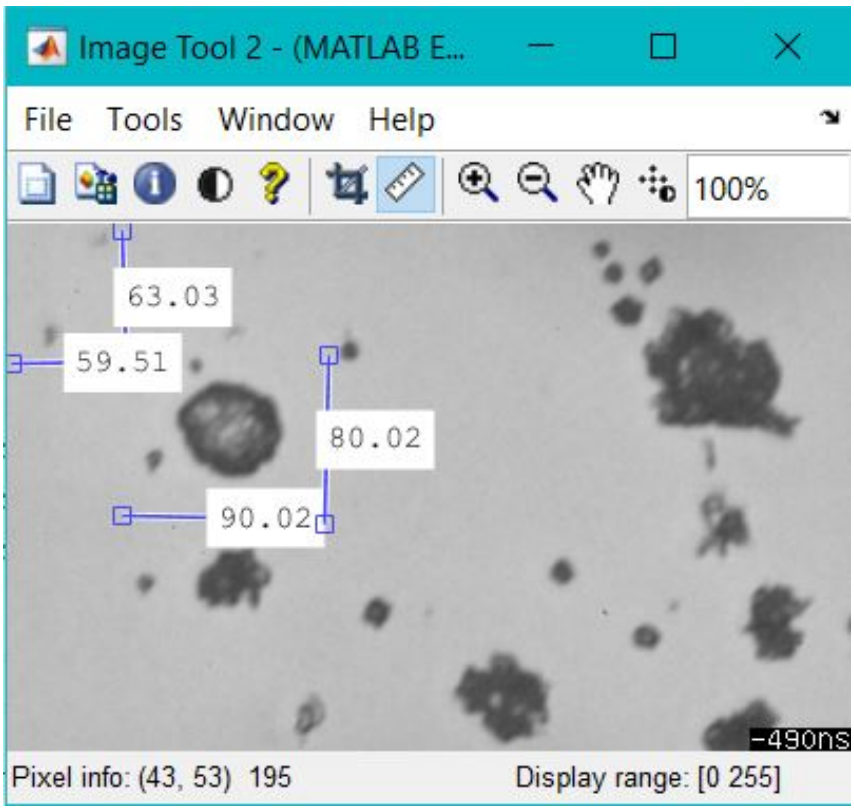

Figure 4.5: Manual selection of region containing (anti)bubble of interest.

In order to segment the antibubble from the background in each cropped frame, the greyscale image was converted to binary format. The grey-level window slicing technique was used to do this. This technique uses a given threshold brightness value to determine whether each pixel should be converted to black or white. All pixels above the threshold value are made white, while all pixel below the threshold value are made black [44].

A MATBLAB® automatic, adaptive, thresholding technique, known as Otsu's method, was used to obtain the threshold value used for the binary conversion [54]. This

automatic thresholding technique was chosen as it is both more robust and consistent than manually selecting the threshold value for each image. Otsu's method effectively steps through all the threshold possibilities, takes into account the weight of the background and foreground distributions, and finds the threshold with the least in-class variance (σ_{icv}). This is achieved by iteratively setting the threshold value to each greyscale value in the image and determining both the average greyscale value and number of pixels below (N_{bt}) and above (N_{at}) the given threshold value. The variance for both the greyscale values below (σ_{bt}) and above (σ_{at}) the threshold values are then used, along with the weighted number of pixels in each rage, to calculate the in-class variance:

$$\sigma_{\mathrm{icv}} = \sqrt{{\sigma_{\mathrm{at}}}^2 \cdot \frac{N_{\mathrm{at}}}{N_{\mathrm{tot}}} + {\sigma_{\mathrm{bt}}}^2 \cdot \frac{N_{\mathrm{bt}}}{N_{\mathrm{tot}}}} \tag{4.1}$$

In the rare instances that this thresholding method didn't work, often owing to a cropped image that did not allow for an accurate weighted balance of pixels on either side of the greyscale value, a threshold value was manually chosen.

For each cropped image any black pixels that were surrounded by white pixels were converted to white pixels. This was to account for the darker centre pixels of (anti)bubbles that were below the threshold value in the greyscale image and would otherwise have been converted to black pixels. Additionally any white pixel groups that were in contact with the frame of the image, and therefore not in complete view, were also converted to black pixels and ignored.

Each antibubble in an image was then automatically identified and labelled as an object using the BWLABEL MATLAB® function, which searched for and labelled groups of white connected pixels as numbered objects. Figure 4.6 below shows the steps taken to convert the antibubbles in the greyscale cropped image, to a labelled object.

In most cases only a single object was measured at a time, so as to ensure that antibubble objects did not get swapped across frames. This could happen as antibubbles oscillated in size and shifted slightly in location during each experiment and the objects were numbered according to their pixel position on the x-axis. If two antibubbles occupied very similar x-axis positions within the frame, their position in the object order could easily become swapped between frames if one bubble's outer radius shifted in location more than the other. In cases where the antibubble objects were far enough apart to ensure no overlapping or change in order could occur, the size of multiple antibubbles could be recorded at once as shown in Figure 4.7, where two different antibubbles have been identified as two separate objects.

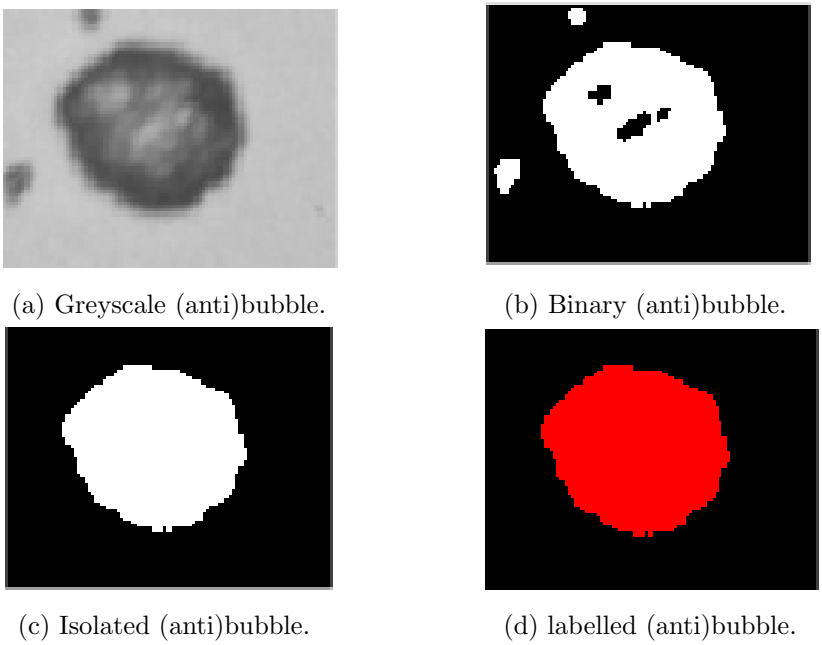

(a) Greyscale (anti)bubble.

(b) Binary (anti)bubble.

(c) Isolated (anti)bubble.

(d) labelled (anti)bubble.

Figure 4.6: Automated segmentation and antibubble size detection process on an (anti)bubble.

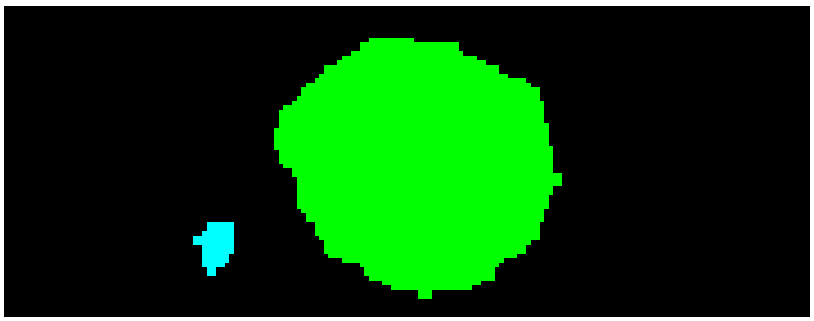

Figure 4.7: Two separate (anti)bubble objects, visually distinguished by colour.

The area of each antibubble was measured by counting the number of white pixels within each identified object. From the area the radius could be calculated using the following standard equation of a circle $\left(R = \sqrt{\frac{A}{\pi}}\right)$. As the ratio of pixel size to size in reality was know, the area of each antibubble could be calculated in micrometers.

For each antibubble measured within each video, an array of radii per frame was created. A structure array was then created containing the radius measurement array and property descriptions of each (anti)bubble. The properties included; (anti)bubble type, ultrasound amplitude exposed to, the number of times the (anti)bubbles had been exposed to ultrasound and the equilibrium, maximum, minimum and final radii.

4.4 Post-processing and analysis

This section details the post-processing of the radius(time) data captured from the image processing. The points of significance in this study are first described in detail below before the use of them is discussed.

To illustrate the significant points of interest, an example of the ultrasound pulse generated and the corresponding antibubble radius(time) curve is given in Figures 4.8 and 4.9. The radius(time) curve has been annotated with the points of interest that have been used in the quantitative analysis of the difference between each (anti)bubble type. Selected frames of the footage, correlating to the significant points highlighted in the given radius(time) curve, are shown in Figure 4.10. These images present the visual radius changes observed and discussed for each experiment. The particular antibubble used in this example is of type AB1 and was subjected to ultrasound at an amplitude of 1 V and a peak negative pressure of 200 kPa.

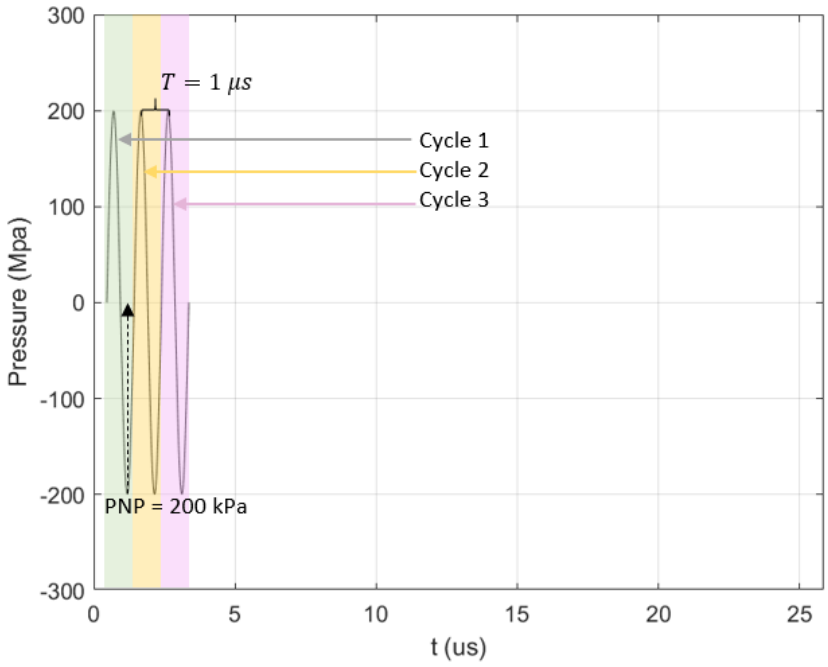

Figure 4.8: Visual representation of a 1 V amplitude (200 kPa peak negative pressure) ultrasound pulse within the full timespan of an experiment. The pulse consists of three ultrasound cycles with a centre frequency (f_c) of 1 MHz and a dominant period (T) of 1 μs. Each of the cycles within the pulse are shaded a different colour, with the first cycle shaded in green, the second in yellow and the third in magenta.

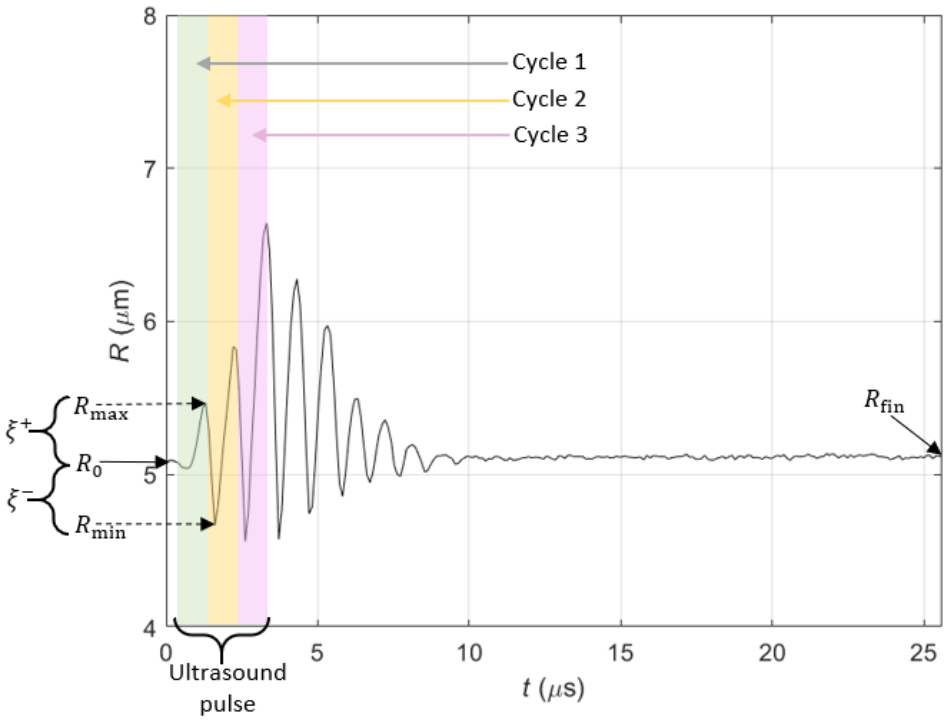

Figure 4.9: The radius(time) (R(t)) curve of a standard antibubble during and after ultrasound exposure at 1 V. The shaded area is the time over which the single pulse of ultrasound was applied, with the first cycle shaded in green, the second in yellow and the third in magenta. The position of the radius measurements discussed in this dissertation are also shown, these include: the initial radius (R_0), the maximum radius during the first cycle of ultrasound ($R_{\max}$), the minimum radius measurement after the first cycle ($R_{\min}$) and the final radius (R_{fin}). The amount of positive and negative excursion from the initial radius value owing to the onset of the first cycle of ultrasound is marked by ξ^+ and ξ^- respectively.

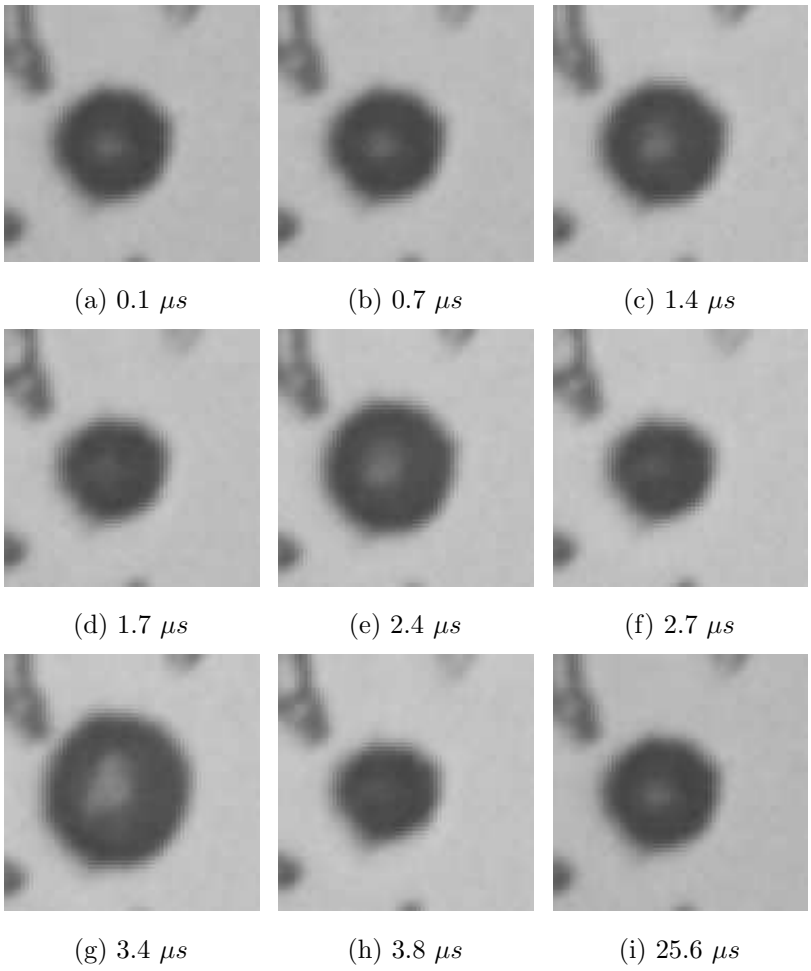

(a) 0.1 μs (b) 0.7 μs (c) 1.4 μs

(d) 1.7 μs (e) 2.4 μs (f) 2.7 μs

(g) 3.4 μs (h) 3.8 μs (i) 25.6 μs

Figure 4.10: Individual frames that show the change in radius of an antibubble under sonication at 1V. The points of interest shown are: (a) the equilibrium radius prior to sonication (R_0), (b) the slight negative excursion as ultrasound in applied, (c) the maximum radius owing to positive excursion during the first cycle ($R_{\max}$), (d) the minimum radius after the first cycle of ultrasound ($R_{\min}$), (e–h) depict the succeeding maximum and minim positive excursion and negative excursion points whilst still under sonication, (i) shows the radius over 200 μs after sonication (R_{fin}). The time lapsed from the start of the experiment is given underneath each frame.

Footage of (anti)bubbles during ultrasound exposure at 200 kPa as well as at 1 MPa was used to investigate the expansion-only hypothesis of antibubbles. Only AB1 and REF were used in the quantitative investigation of this hypothesis, as there were far fewer AB2 antibubble experiments and therefore significantly fewer AB2 antibubbles than that of AB1 and REF. The decision to only compare AB1 and REF antibubbles was also made to simplify the scatter plot diagrams, as too many scatter plot points would make the graphs challenging to read.

A scatter plot showing the relationship between the maximum radius of (anti)bubbles during the first cycle of sonication and the equilibrium radius prior to sonication was used to investigate the effect that size of initial (anti)bubble radius had on (anti)bubble positive excursion. Regression lines were added which fit the data to a standard first order polynomial function, ie. $y = mx + c$. While this graph showed that the radii increased in size after the first cycle of ultrasound, the amount by which they increased was not apparent. A scatter plot of the amount of positive excursion ($\xi^+ = R_{\max} - R_0$) compared to the equilibrium radii of each (anti)bubble was created to better show the amount of positive excursion each (anti)bubble underwent.

A similar plot was made to show the relationship between the minimum radius of (anti)bubbles during the first cycle and the equilibrium radius prior to sonication was used to investigate the effect that initial antibubble radius had on antibubble negative excursion. The corresponding scatter plot of the amount of negative excursion ($\xi^- = R_{\min} - R_0$) compared to the equilibrium radii was created to better show the amount of negative excursion each (anti)bubble underwent.

The oscillation asymmetry ($\xi^+ - \xi^- = R_{\max} + R_{\min} - 2R_0$), is the total change in (anti)bubble radius owing to the positive excursion and negative excursion that took place during the first cycle of ultrasound. This gives a clear indication of the symmetry of oscillation as a zero result indicates symmetric oscillation, a negative result indicates more negative excursion than positive excursion and a positive result indicates the inverse. This value was calculated for each (anti)bubble and compared against the corresponding equilibrium radius of each (anti)bubble in a scatter plot. This graph allowed for the symmetry of oscillation to be observed.

To investigate the prolonged effect of exposure the equilibrium radius of (anti)bubbles of type AB1 and REF were compared to the radius 20 μs after three cycles of ultrasound exposure (R_{fin}). No 5 V comparison is given for this section owing to the fact that all the (anti)bubbles exposed to ultrasound of 5 V amplitude fragmented during their first cycle of sonication and thus has no final values.

For the investigation of antibubble reliability and stability, only (anti)bubbles that had been exposed to ultrasound with a peak negative pressure of 200 kPa (1 V) were considered, as (anti)bubble fragmentation occurred during exposure to the first cycle of each 1 MPa ultrasound pulse. Additionally only bubbles that were accurately measurable for the entire 25.6 μs experiment were considered as stability after sonication was also observed.

To investigate the reliability of antibubbles, the radius(time) curves of three different (anti)bubbles of the same type, with near identical initial radii, were plotted on one graph. This was done multiple times for different initial radii. To compare the stability and reliability, radius(time) curves of an AB1, AB2 and REF (anti)bubble of near identical initial radii were plotted on a single graph. Corresponding plots of the Fast Fourier transforms (FFT) of these plots were produced to investigate whether any differences, that could not be visually seen in the time domain, occurred.

The effect of prior exposure to an ultrasound pulse was also investigated by plotting the radius(time) curves generated as a results of the first, second and third ultrasound pulse applied to the same antibubble. Corresponding FFT plots of these graphs were also plotted and analysed.

For the fragmentation analysis, instances of fragmentation were manually found in the footage and studied. Specific frames comparing the responses of antibubbles and bubbles exposed to signal amplitudes of 1 V and 5 V were chosen and analysed in detail. An antibubbles that exhibited abnormal oscillation behaviour under sonication was also identified and discussed.

Chapter 5

Results

This chapter presents the results of the post processing analysis discussed in the previous chapter. For consistency throughout this chapter blue, red and black are used to indicate (anti)bubbles of type AB1, AB2 and REF respectively. To start the chapter off, a summary of the number and distribution of (anti)bubbles is discussed. Following this, the results for the investigations into the expansion-only hypothesis of antibubbles, antibubble oscillation reliability and stability as well as antibubble fragmentation are presented.

5.1 Distribution of antibubble types

Footage of a total of 333 individual antibubbles during exposure to a single pulse of ultrasound were analysed from 65 recorded experiments. Excluded from these totals are the (anti)bubbles that were not accurately measurable at any point within the first 4 μs of each experiment. In addition, 21 of the experiments were repeated twice on some (anti)bubble sets. This was done to determine the effect of three consecutive pulses of ultrasound on each (anti)bubble type, ultimately resulting in the analysis of a further 42 videos, in which a total 172 antibubbles were analysed.

Of the footage showing (anti)bubbles under sonication at a peak negative pressure of 200 kPa, 111 reference bubbles, 81 antibubbles of type AB1 and 51 antibubbles of type AB2 met the criteria for analysis. Less than a third of the experimental footage was of (anti)bubbles under sonication at a peak negative pressure of 1 MPa. A total of 33 reference bubbles, 37 antibubbles of type AB1 and 20 antibubbles of type AB2 were fully measurable during the first 4 μs of their respective experiments.

The image processing selection criteria for the antibubbles in the repeated experiments additionally included the specification that the antibubbles must be fully visible throughout the full duration of all three experiments. Ultimately a total of 83 (anti)bubbles, 18 REF bubbles, 40 AB1 antibubbles and 25 AB2 antibubbles met this criteria. (Anti)bubbles that were exposed to multiple pulses are only counted once in the distribution graphs in Figure 5.1 below.

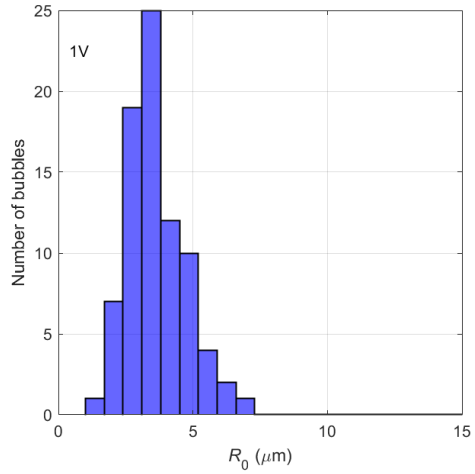

(a) AB1 sonicated at 1 V.

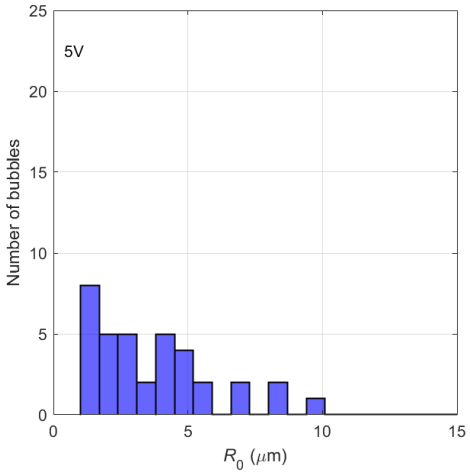

(b) AB1 sonicated at 5 V.

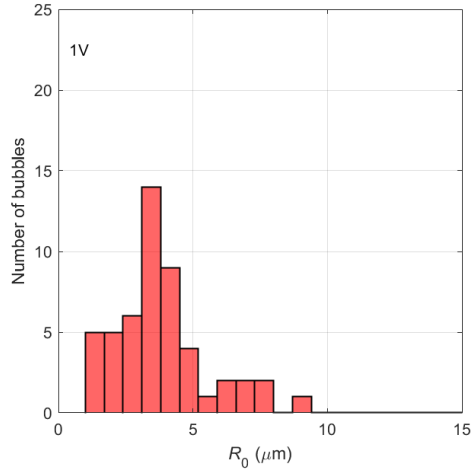

(c) AB2 sonicated at 1 V.

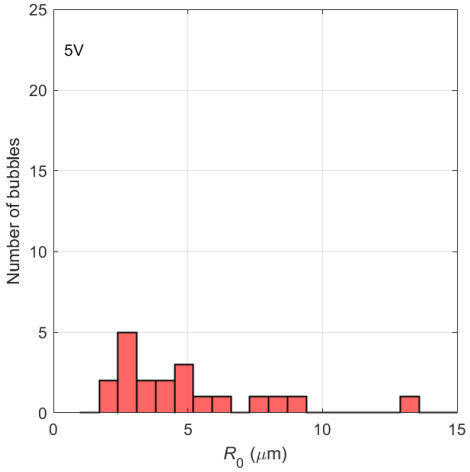

(d) AB2 sonicated at 5 V.

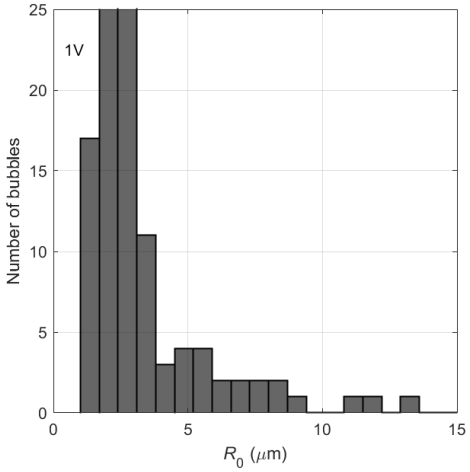

(e) REF sonicated at 1 V.

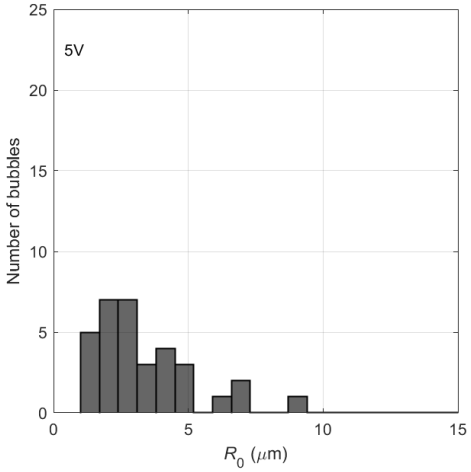

(f) REF sonicated at 5 V.

Figure 5.1: Histograms showing the number of processed bubbles grouped by equilibrium radii for antibubble type AB1 (blue), AB2 (red) and REF (grey). The antibubbles that were exposed to a signal amplitude of 1 V are shown on the left and those that were exposed to a signal amplitude of 5 V are shown on the right.

5.2 Expansion-only hypothesis

The results of the expansion-only hypothesis investigation are given in this section. The expansion, negative excursion and oscillation asymmetry of antibubbles and bubbles during the first cycle of ultrasound at amplitudes of 1 V and 5 V are compared. Finally, the lasting impact of exposure to a single ultrasound pulse with a peak negative pressure of 200 kPa, on antibubbles and bubbles is compared. The least squares regression fit of the data for each (anti)bubble type, within each graph, has been included in each figure. It should be noted that these regression lines have been extended for easier visualization and that the fit should only be considered for (anti)bubbles greater than 0 μm in size.

Figure 5.2 shows the equilibrium radii vs the maximum radii during the first cycle of ultrasound at amplitudes of 1 V and 5 V for AB1 antibubbles (blue circles) and REF bubbles (black crosses). The least squares regression lines of each (anti)bubble at the respective ultrasound amplitudes are also given. Figure 5.3 presents the corresponding expansion of each of the antibubbles in Figure 5.2.

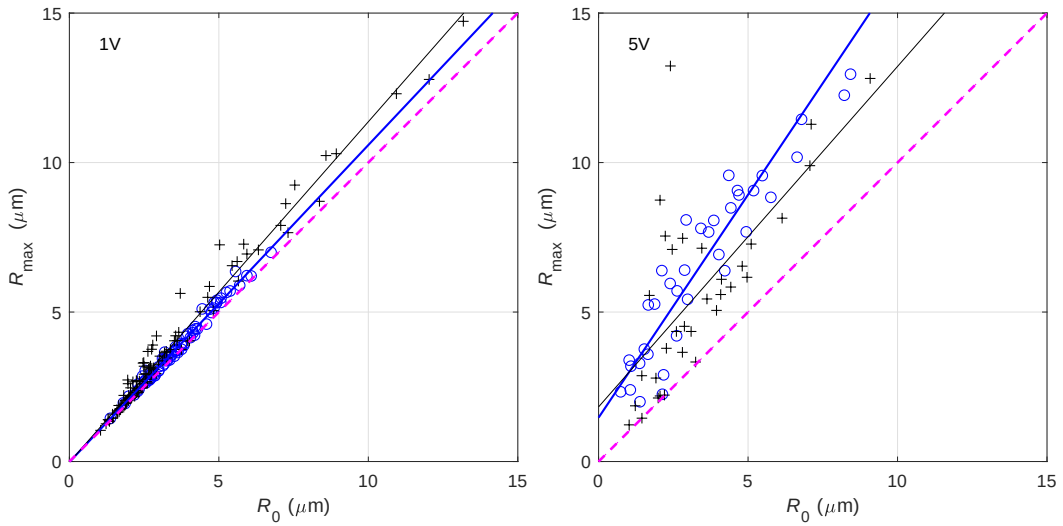

(a) (b)

Figure 5.2: Equilibrium radius (R_0) vs maximum positive excursion radius after the first cycle for AB1 antibubbles (blue circles) and REF bubbles (black crosses) at both (a) 1 V and (b) 5 V. The dashed purple line corresponds to $R_{\max} = R_0$, and the thick blue and thin black lines refer to the least squares regression lines of AB1 and REF respectively.

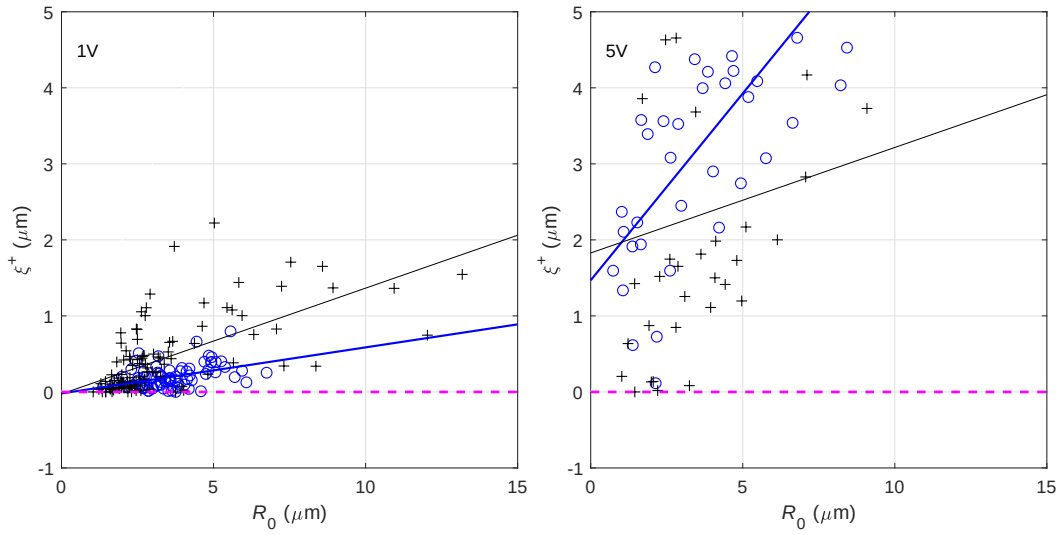

(a) (b)

Figure 5.3: Equilibrium radius (R_0) vs positive excursion (ξ^+) during the first cycle for antibubbles AB1 (blue circles) and bubbles REF (black crosses) at both (a) 1 V and (b) 5 V. The thick blue and thin black lines refer to the least squares regression lines of AB1 and REF respectively.The dotted purple line represent zero positive excursion (ξ^+=0).

AB1 antibubbles show a minimal change in size during the first cycle of ultrasound at amplitude 1 V with a polynomial of:

$$R_{\max} = 1.06R_0 - 0.0196, R_0 > 0, \tag{5.1}$$

with corresponding expansion function:

$$\xi^+ = 0.0605R_0 - 0.0196, R_0 > 0. \tag{5.2}$$

Reference bubbles experience a fractional, but definite comparative increase in size when exposed to the same ultrasonic conditions, with a polynomial function of:

$$R_{\max} = 1.14R_0 - 0.0271, R_0 > 0, \tag{5.3}$$

and corresponding expansion function:

$$\xi^+ = 0.139R_0 - 0.0271, R_0 > 0. \tag{5.4}$$

It is clear from Figures 5.2 and 5.3, that when exposed to ultrasound at an amplitude of 5 V AB1 antibubbles, which have a linear regression function of:

$$R_{\max} = 1.49R_0 + 1.47, R_0 > 0, \tag{5.5}$$

and corresponding expansion function of:

$$\xi^{+} = 0.491R_0 + 1.47, R_0 > 0, \tag{5.6}$$

expand substantially more than REF bubbles do. The linear regression function for the reference bubble results is:

$$R_{\max} = 1.14R_0 + 1.83, R_0 > 0, \tag{5.7}$$

with corresponding expansion function:

$$\xi^{+} = 0.139R_0 + 1.83, R_0 > 0. \tag{5.8}$$

Figure 5.4 shows the equilibrium radii vs the minimum radii during the first cycle of ultrasound at amplitudes of 1 V and 5 V for AB1 antibubbles (blue circles) and REF bubbles (black crosses). The least squares regression lines of each (anti)bubble at the respective ultrasound amplitudes are also shown. Figure 5.5 shows the corresponding negative excursion of each of the antibubbles in Figure 5.4.

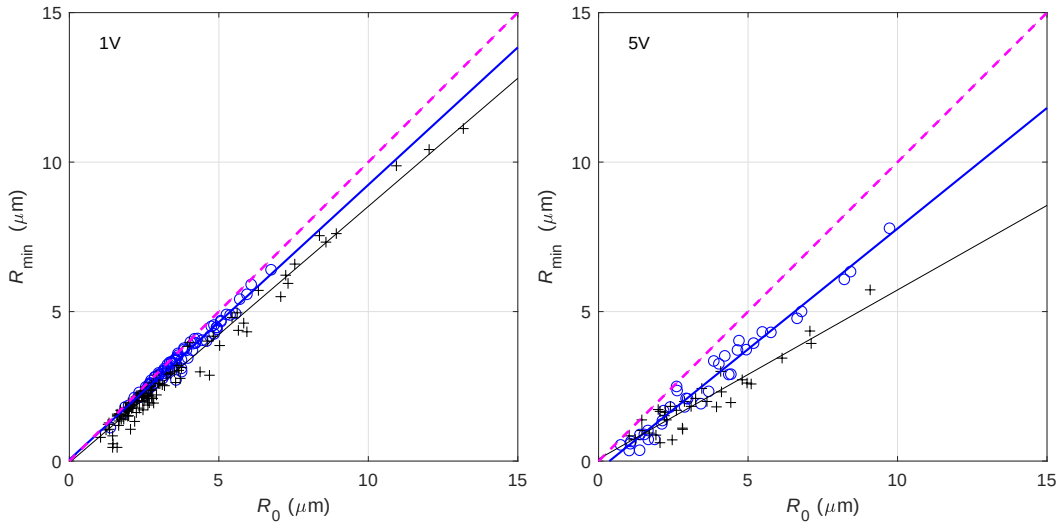

(a) (b)

Figure 5.4: Equilibrium radius (R_0) vs minimum negative excursion radius after the first cycle for AB1 antibubbles (blue circles) and REF bubbles (black crosses) at both (a) 1 V and (b) 5 V. The dashed purple line corresponds to $R_{\min} = R_0$, and the thick blue and thin black lines refer to the least squares regression lines of AB1 and REF respectively.

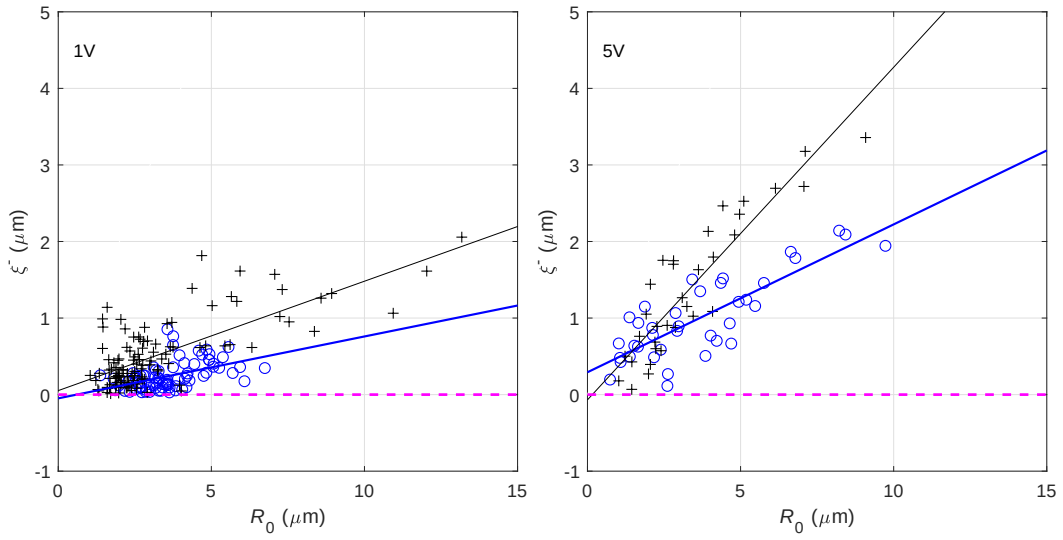

(a) (b)

Figure 5.5: Equilibrium radius (R_0) vs negative excursion (ξ^-) after the first cycle for antibubbles AB1 (blue circles) and bubbles REF (black crosses) at both (a) 1 V and (b) 5 V. The thick blue and thin black lines refer to the least squares regression lines of AB1 and REF respectively. The dotted purple line represent zero negative excursion (ξ^-=0).

Similarly to their expansion behaviour under exposure at 1 V, AB1 antibubbles show a minimal change in size owing to negative excursion during the first cycle of ultrasound, with a polynomial best fit function of:

$$R_{\min} = 0.919R_0 + 0.0488, R_0 > 0, \tag{5.9}$$

and a corresponding negative excursion function of:

$$\xi^- = 0.0808R_0 - 0.0488, R_0 > 0. \tag{5.10}$$

REF bubbles once again show a fractional, but comparatively large change in size, this time during negative excursion, with polynomial equation:

$$R_{\min} = 0.857R_0 - 0.0523, R_0 > 0, \tag{5.11}$$

with corresponding negative excursion function:

$$\xi^- = 0.142R_0 + 0.0523, R_0 > 0. \tag{5.12}$$

In contrast to the expansion graphs, the relationship between AB1 and REF negative excursion was exaggerated for the samples that had been exposed to a 5 V amplitude

ultrasound pulse. AB1 antibubbles exhibit negative excursion, a trend confirmed by the least squares regression polynomial:

$$R_{\min} = 0.807R_0 - 0.292, R_0 > 0, \tag{5.13}$$

and corresponding negative excursion function:

$$\xi^- = 0.193R_0 + 0.292, R_0 > 0. \tag{5.14}$$

REF bubbles contract far more however, with a least squares regression polynomial of:

$$R_{\min} = 0.566R_0 + 0.0686, R_0 > 0, \tag{5.15}$$

and corresponding negative excursion function:

$$\xi^- = 0.434R_0 - 0.0686, R_0 > 0. \tag{5.16}$$

Figure 5.6 shows the equilibrium radii vs the oscillation asymmetry as a result of the first cycle of ultrasound at amplitudes of 1 V and 5 V for AB1 antibubbles (blue circles) and REF bubbles (black crosses). The least squares regression lines of each (anti)bubble type under the respective ultrasonic conditions are also shown and can be compared against the purple dotted line which represents perfectly symmetrical excursion.

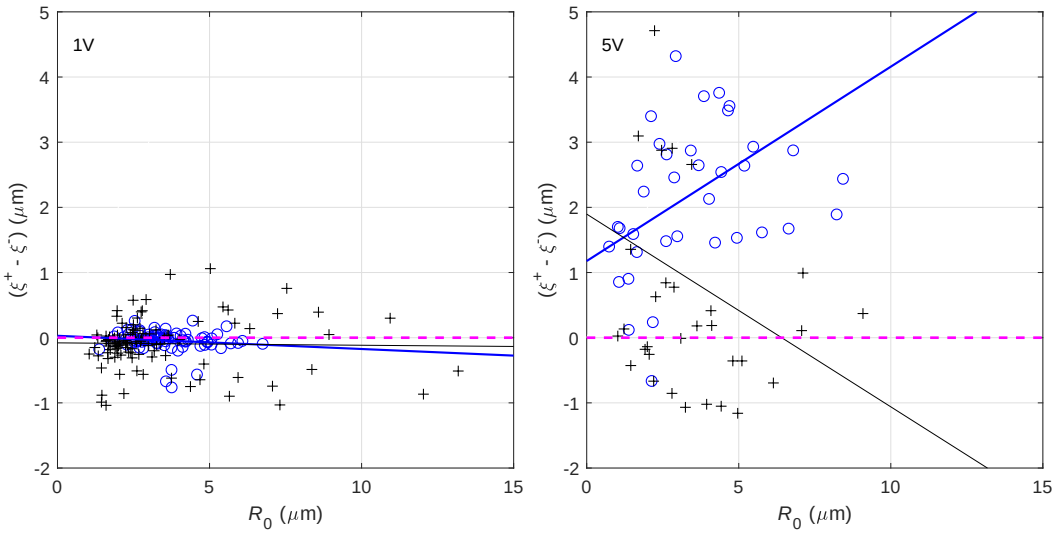

(a) (b)

Figure 5.6: Equilibrium radius (R_0) vs oscillation asymmetry ($\xi^+ - \xi^-$) as a result of a single cycle of ultrasound for AB1 antibubbles (blue circles) and REF bubbles (black crosses) at both (a) 1 V and (b) 5 V. The dotted purple line represents perfectly symmetrical excursion which is expressed as $(\xi^+ - \xi^-) = 0$. The thick blue and thin black lines refer to the least squares regression lines of AB1 and REF respectively.

At a peak acoustic amplitude of 1 V antibubbles are shown to contract very minimally more than they expand. This asymmetry is negligible, with a least squares regression polynomial of:

$$(\xi^+ - \xi^-) = -0.0202R_0 + 0.0293, R_0 > 0. \tag{5.17}$$

Table 5.1 shows the expected negative excursion, positive excursion and oscillation asymmetry based on (5.17) for antibubbles within the range of 2 μm to 10 μm. This range was chosen as most of the antibubbles examined were within this range. The percentage of expected negative excursion, positive excursion and oscillation asymmetry antibubbles relative to their equilibrium radii during exposure to ultrasound is also given.

Table 5.1: Expected positive excursion, negative excursion, oscillation asymmetry and the respective percentages thereof for AB1 antibubbles relative to equilibrium radii during exposure to ultrasound with a peak negative pressure of 200 kPa.

$R_0(\mu\mathbf{m})$	$\xi^+(\mu\mathbf{m})$	**% of** R_0	$\xi^-(\mu\mathbf{m})$	**% of** R_0	$\xi^+ - \xi^-(\mu\mathbf{m})$	**% of** R_0
2.00	0.102	5.10	0.113	5.65	-0.011	-0.55
3.00	0.163	5.43	0.194	6.47	-0.031	-1.03
4.00	0.224	5.60	0.275	6.88	-0.051	-1.28
5.00	0.285	5.70	0.356	7.12	-0.071	-1.42
6.00	0.346	5.77	0.437	7.28	-0.091	-1.52
7.00	0.407	5.81	0.518	7.40	-0.111	-1.59
8.00	0.468	5.85	0.599	7.49	-0.131	-1.64
9.00	0.529	5.88	0.680	7.56	-0.151	-1.68
10.0	0.290	5.90	0.761	7.61	-0.171	-1.71
Averages						
6.00	0.346	5.67	0.437	7.05	-0.091	-1.38

REF bubbles also show a minute amount of asymmetry, that is clearly negligible from the least squares regression polynomial:

$$(\xi^+ - \xi^-) = -0.00366R_0 - 0.0794, R_0 > 0. \tag{5.18}$$

Table 5.2 shows the expected negative excursion, positive excursion and oscillation asymmetry based on (5.18) for reference bubbles within the range of 2 μm to 10 μm. The percentage of expected negative excursion, positive excursion and oscillation

asymmetry of bubbles relative to their equilibrium radii during exposure to ultrasound is also given.

Table 5.2: Expected positive excursion, negative excursion, oscillation asymmetry and the respective percentages thereof for reference bubbles relative to equilibrium radii during exposure to ultrasound with a peak negative pressure of 200 kPa.

$R_0(\mu\mathbf{m})$	$\xi^+(\mu\mathbf{m})$	% **of** R_0	$\xi^-(\mu\mathbf{m})$	% **of** R_0	$\xi^+ - \xi^-(\mu\mathbf{m})$	% **of** R_0
2.00	0.251	12.55	0.336	16.80	-0.087	-4.34
3.00	0.390	13.00	0.478	15.93	-0.090	-3.01
4.00	0.529	13.23	0.620	15.50	-0.094	-2.35
5.00	0.668	13.36	0.762	15.24	-0.098	-1.95
6.00	0.807	13.45	0.904	15.07	-0.101	-1.69
7.00	0.946	13.51	1.046	14.94	-0.105	-1.50
8.00	1.085	13.56	1.188	14.85	-0.109	-1.36
9.00	1.224	13.60	1.330	14.78	-0.112	-1.25
10.0	1.363	13.63	1.472	14.72	-0.116	-1.16
Averages						
6.00	0.807	13.32	0.904	15.31	-0.101	-2.07

At a peak negative acoustic pressure of 1 MPa AB1 antibubbles exhibit asymmetric oscillation with antibubbles showing significantly higher positive excursion than negative excursion. The highly asymmetric oscillatory response of AB1 antibubble at an acoustic amplitude of 5 V appears to be confirmed by a least square regression polynomial of:

$$(\xi^+ - \xi^-) = 0.298R_0 + 1.18, R_0 > 0. \tag{5.19}$$

Table 5.3 shows the expected negative excursion, positive excursion and oscillation asymmetry based on (5.19) for reference bubbles within the range of 2 μm to 10 μm. The percentage of expected negative excursion, positive excursion and oscillation asymmetry of antibubbles relative to their equilibrium radii during exposure to ultrasound is also given. Here oscillation asymmetry is clearly always positive, although the percentage oscillation asymmetry appears to reduce as bubble size increases.

Table 5.3: Expected positive excursion, negative excursion, oscillation asymmetry and the respective percentages thereof for AB1 antibubbles relative to equilibrium radii during exposure to ultrasound with a peak negative pressure of 1 MPa.

$R_0(\mu\mathbf{m})$	$\xi^+(\mu\mathbf{m})$	% **of** R_0	$\xi^-(\mu\mathbf{m})$	% **of** R_0	$\xi^+ - \xi^-(\mu\mathbf{m})$	% **of** R_0
2.00	2.451	122.55	0.678	33.90	1.772	88.60
3.00	2.942	98.07	0.871	29.03	2.070	69.00
4.00	3.433	85.83	1.064	26.60	2.368	59.20
5.00	3.924	78.48	1.257	25.14	2.666	53.32
6.00	4.415	73.58	1.450	24.17	2.964	49.40
7.00	4.906	70.09	1.643	23.47	3.262	46.60
8.00	5.397	67.46	1.836	22.95	3.560	44.50
9.00	5.888	65.42	2.029	22.54	3.858	42.87
10.0	6.379	63.79	2.222	22.22	4.156	41.56
Averages						
6.00	4.415	80.59	1.450	25.56	2.964	55.01

The linear regression polynomial for the reference bubbles,

$$(\xi^+ - \xi^-) = -0.296R_0 + 1.90, R_0 > 0, \tag{5.20}$$

whilst negative in slope, still shows that for bubbles less than 7 μm in size, positive excursion is greater than negative excursion. It is only for larger reference bubbles that negative excursion becomes larger than positive excursion. Table 5.4 shows this more clearly by giving the average expected negative excursion, positive excursion and oscillation asymmetry based on (5.20) for reference bubbles within the range of 2 μm to 10 μm. The percentage of expected oscillation asymmetry only becomes negative for bubbles with an equilibrium radius larger than 6 μm in size.

Table 5.4: Expected positive excursion, negative excursion, oscillation asymmetry and the respective percentages thereof for reference bubbles relative to equilibrium radii during exposure to ultrasound with a peak negative pressure of 1 MPa.

$R_0(\mu\mathbf{m})$	$\xi^+(\mu\mathbf{m})$	% of R_0	$\xi^-(\mu\mathbf{m})$	% of R_0	$\xi^+ - \xi^-(\mu\mathbf{m})$	% of R_0
2.00	2.106	105.30	0.799	39.95	1.304	65.20
3.00	2.245	74.83	1.233	41.10	1.008	33.60
4.00	2.384	59.60	1.667	41.68	0.712	17.80
5.00	2.523	50.46	2.101	42.02	0.416	8.32
6.00	2.662	44.37	2.535	42.41	0.120	2.00
7.00	2.801	40.01	2.969	42.54	-0.176	-2.51
8.00	2.940	36.75	3.403	42.63	-0.472	-5.90
9.00	3.079	34.21	3.837	42.71	-0.768	-8.53
10.0	3.218	32.18	4.271	42.71	-1.064	-10.64
Averages						
6.00	2.662	53.08	2.535	41.92	0.120	11.04

5.3 Endoskeletal effect on oscillation reliability and stability

This section presents the results of an investigation into whether the endoskeletal content of an antibubble has an effect on it's oscillation whilst under sonication at 1 V. A comparison to antibubbles under exposure to ultrasound at an amplitude of 5 V is not provided in this sections, owing to the fact that all the (anti)bubbles exposed to ultrasound with an amplitude of 5 V fragmented during peak compression of the first cycle of ultrasound and thus could no longer be compared to the equilibrium radii.

The equilibrium radii of antibubbles of type AB1 and REF bubbles are compared in Figure 5.7 to the corresponding radii observed in the final frame of each experiment, about 20 μs after exposure to a single 1 MHz cycle of ultrasound. This gives an indication of the longer term effect of sonication on antibubbles. The less an (anti)bubble changes in equilibrium size after exposure to sonication, the more the period of exposure to ultrasound can be extended without altering the physical, and thus acoustic, properties of the (anti)bubble.

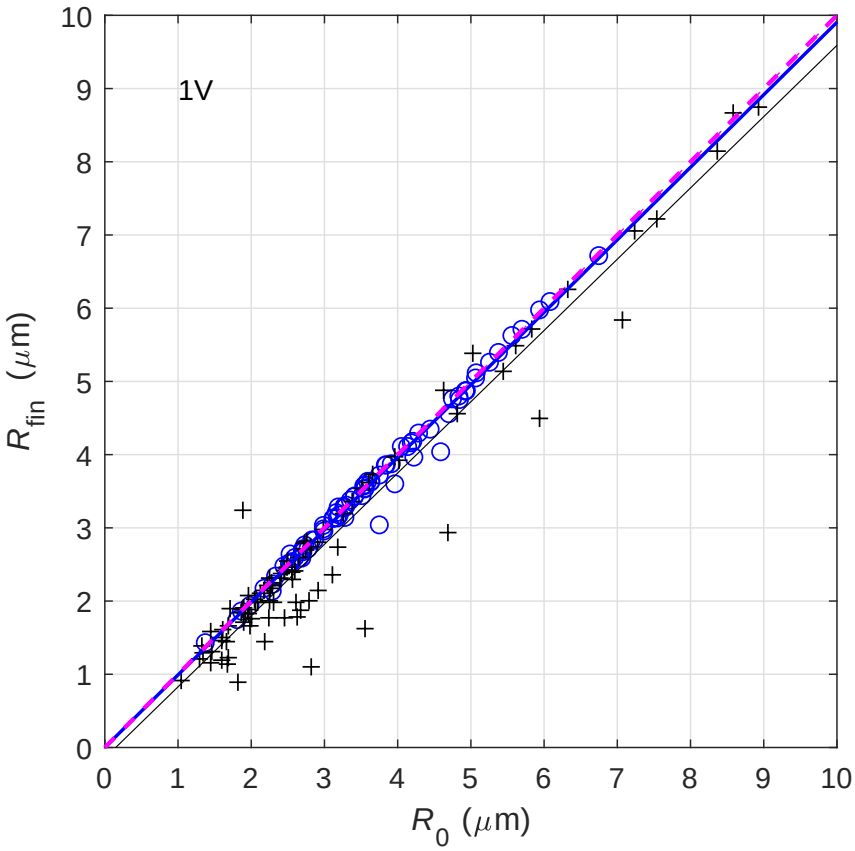

Figure 5.7: Initial radii (R_0) vs final radii (R_{fin}) after a single pulse of ultrasound for AB1 antibubbles (blue circles) and REF bubbles (black crosses) at 1 V. The dotted purple line represents $R_{\text{fin}} = R_0$, whilst the thick blue line and thin black line refer to the least squares regression lines of AB1 and REF respectively.

The linear regression polynomial for AB1 antibubbles under sonication at 1 V,

$$R_{\text{fin}} = 0.990R_0 + 0.00124, R_0 > 0, \tag{5.21}$$

indicates a negligible change in equilibrium radii. When exposed to the same ultrasonic conditions the equilibrium radii of the reference bubbles after sonication show an approximate shrinkage of 0.15 μm, evident in the linear regression polynomial function:

$$R_{\text{fin}} = 0.973R_0 - 0.145, R_0 > 0. \tag{5.22}$$

To investigate reliability further, the radius(time) curves of three different (anti)bubbles of the same type, with near identical initial radii, were plotted against one another. The plots of each antibubble type for two different initial radii ranges can be seen in Figure 5.8. To compare the stability and reliability, radius(time) curves of an AB1,

AB2 and REF (anti)bubble of near identical initial radii were plotted against one another. In Figure 5.9, six different initial radius ranges are shown and compared, with the smallest being $2.5 \pm 0.022\,\mu$m and the largest being $5.409 \pm 0.033\,\mu$m. Corresponding plots of the Fast Fourier transforms (FFT) of these plots can be seen in Figures 5.10 and 5.11.

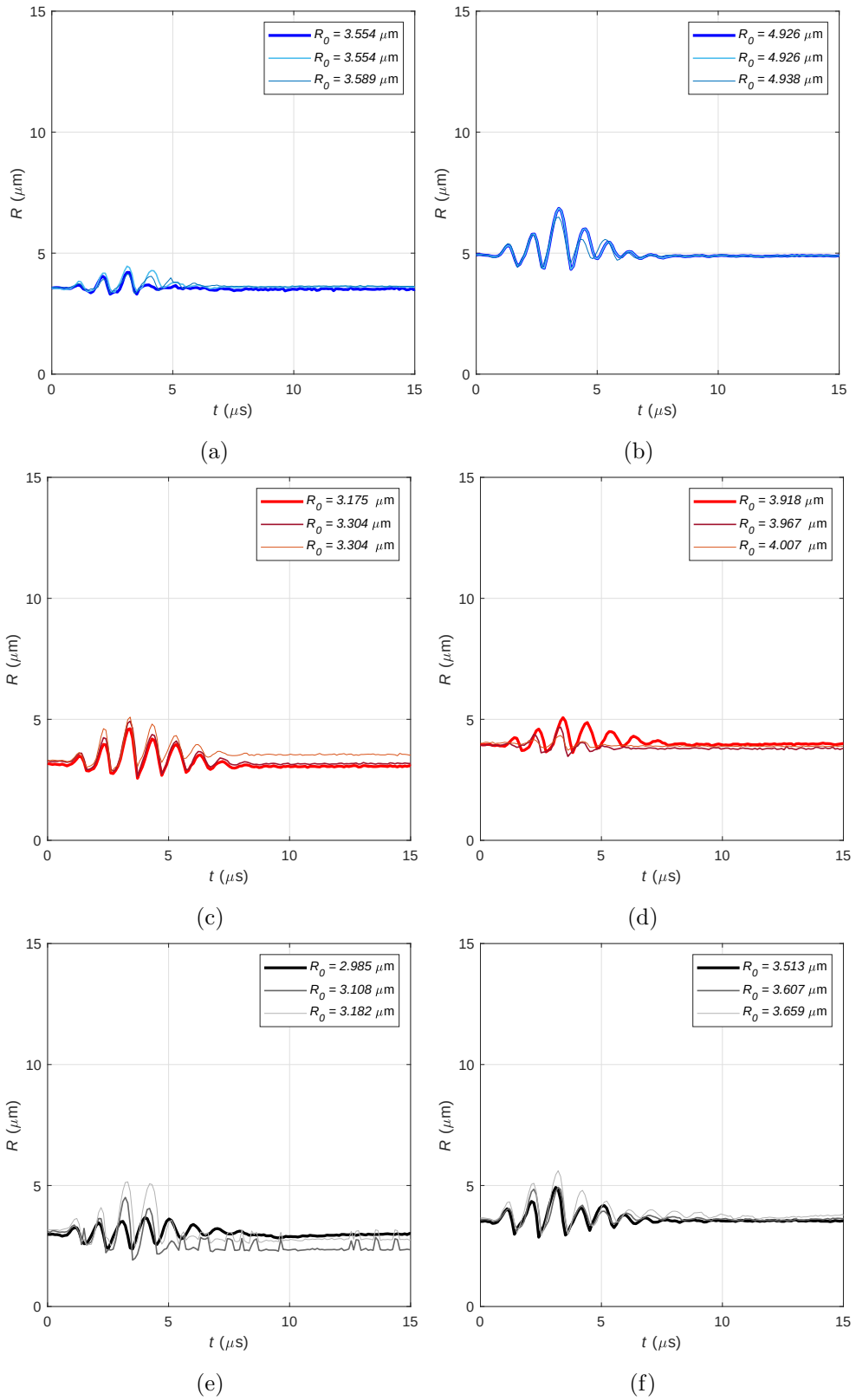

Figure 5.8: R(t) curves comparing similarly sized (anti)bubbles of the same type. AB1 antibubbles are depicted in shades of blue, AB2 antibubbles in shades of red and REF bubbles in shades of grey.

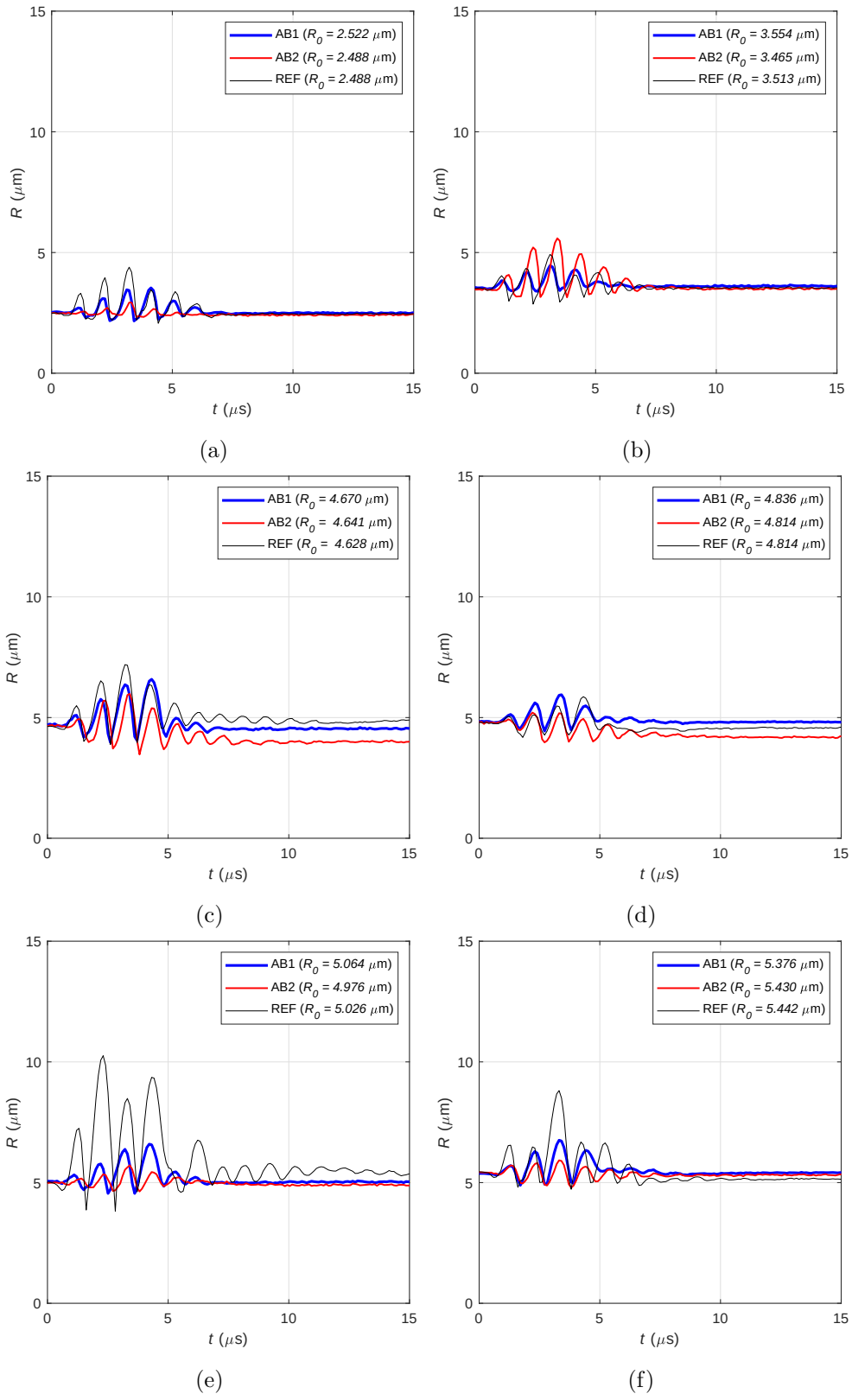

Figure 5.9: R(t) curves comparing similarly sized (anti)bubbles of each type, were AB1 antibubbles are depicted in blue, AB2 antibubbles in red and REF bubbles in black. Each sub-figure illustrates the comparative oscillations for a different range of initial radii.

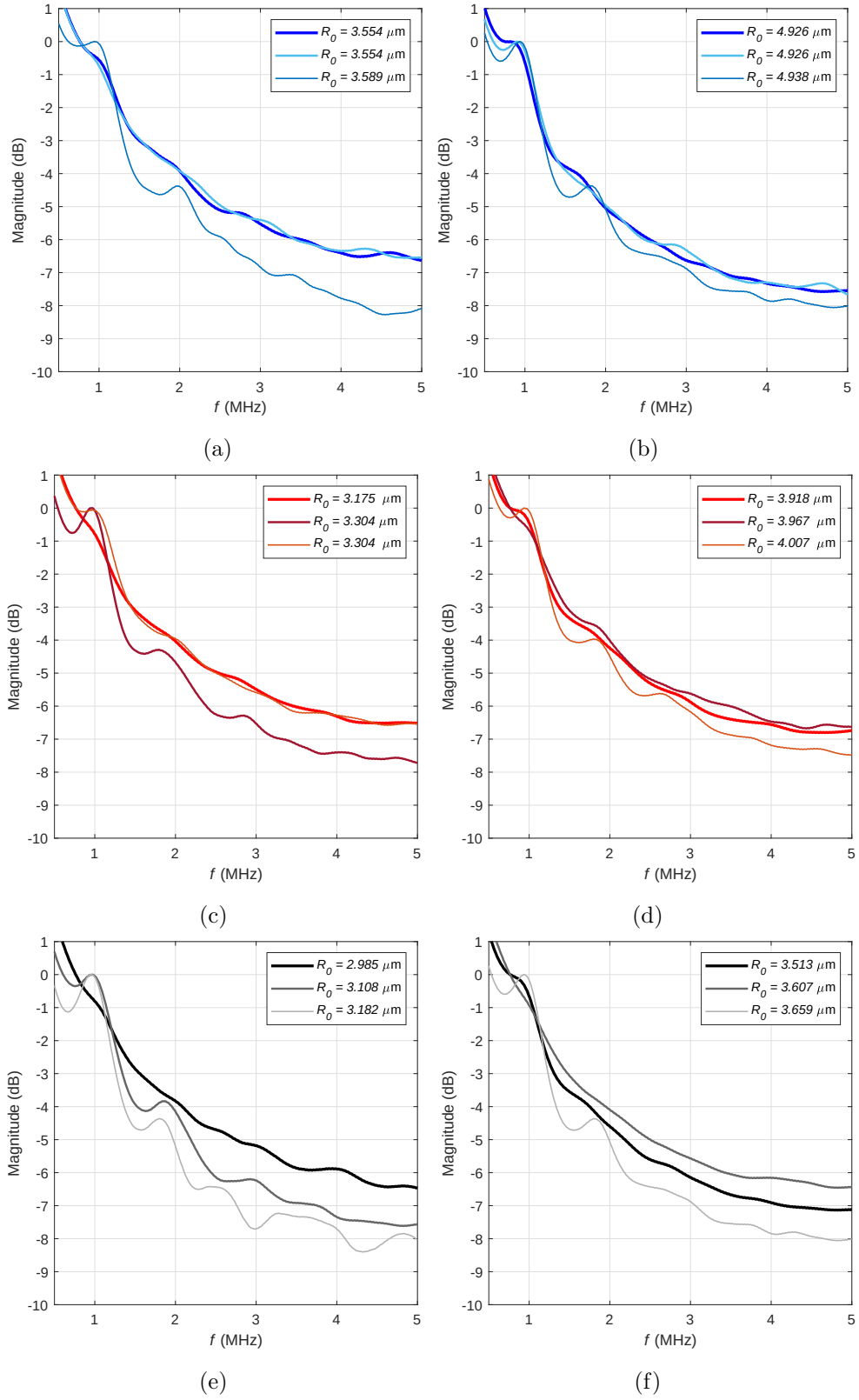

Figure 5.10: Frequency response comparison of similarly sized (anti)bubbles of the same type, where AB1 is depicted in shades of blue, AB2 in shades of red and REF in shades of grey.

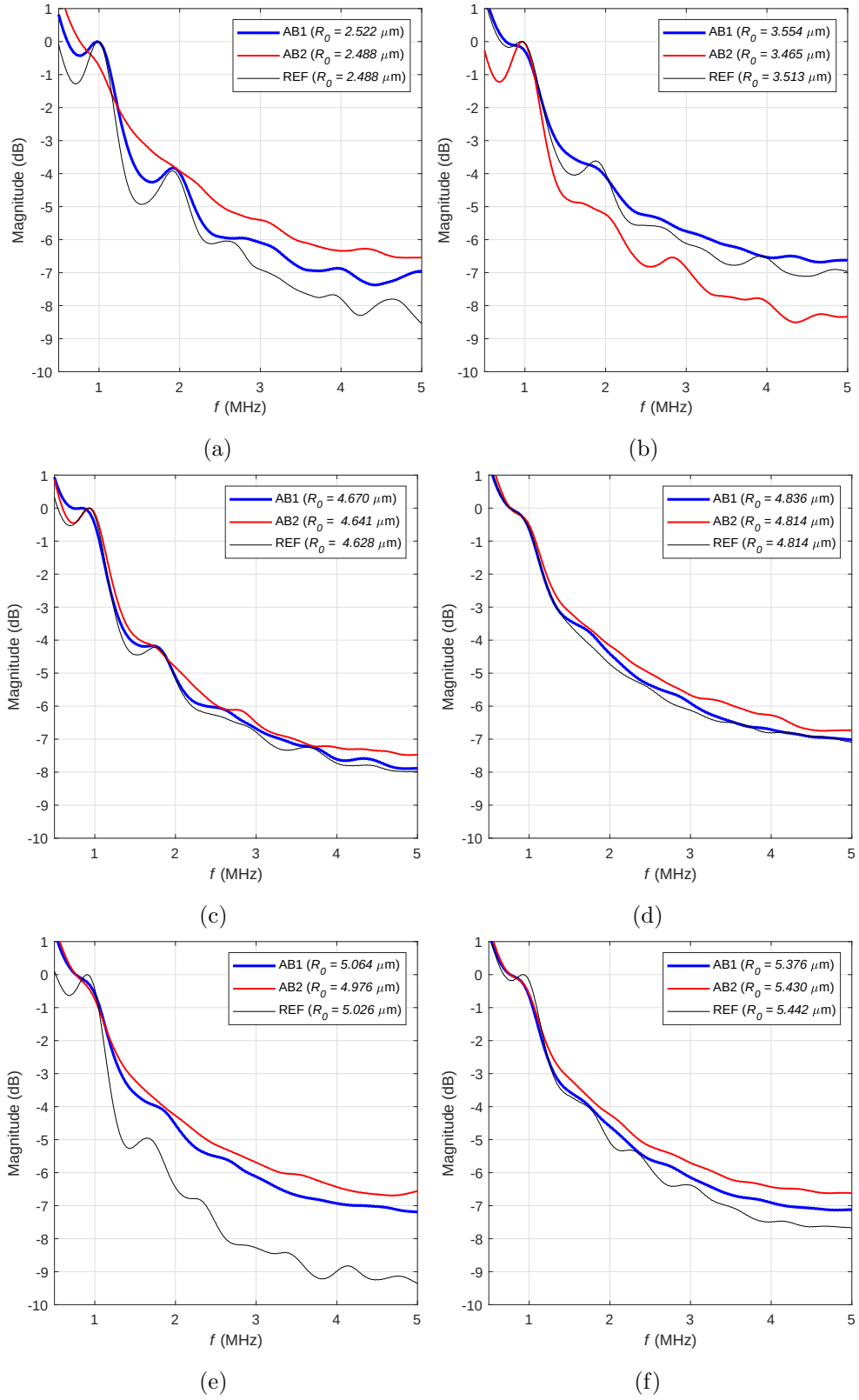

Figure 5.11: Frequency response comparison of similarly sized (anti)bubbles of each type, where AB1 antibubbles are depicted in blue, AB2 antibubbles in red and REF bubbles in black. Each sub-figure illustrates the comparative frequency responses for a different range of initial radii.

Figure 5.8 indicates that antibubbles that are of the same type and of similar size seem to vary minimally in their response to ultrasound, whilst the REF bubbles seem to respond less reliably. All the samples exhibited similar behaviour in the frequency domain shown in Figure 5.10.

Figure 5.9 show that the antibubble with the highest endoskeletal content, AB2, had the lowest oscillatory response in most cases, whilst reference bubbles, which contained no endoskeletal content, often exhibited the highest oscillatory response. The reference bubbles also appear to oscillate for longer than the antibubbles after sonication. All the samples exhibited similar behaviour in the frequency domain shown in Figure 5.11.

The results of an investigation into the effect of multiple pulses of ultrasound on the oscillatory response of (anti)bubbles of type AB1, AB2 and REF are shown in Figures 5.12 to 5.14 below. The frequency response corresponding to the same (anti)bubbles are show in Figures 5.15 to 5.17. In each of these figures, the response owing to the first ultrasound pulse for each type is represented by the standard blue, red or black used to indicate antibubble type AB1, AB2 or REF respectively, the response to the second pulse is represented in dark purple and the third in bottle green.

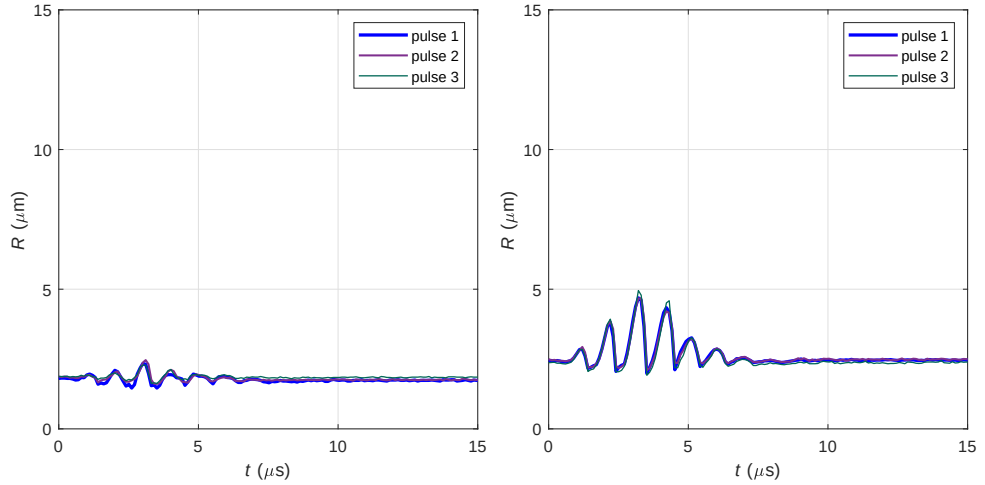

(a) $R_0 = 1.81\,\mu$m.

(b) $R_0 = 2.45\,\mu$m.

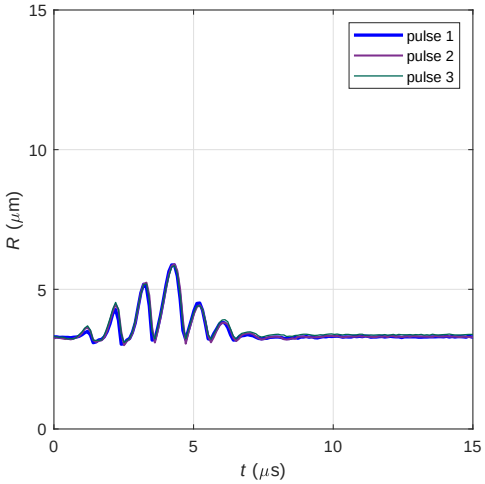

(c) $R_0 = 3.23\,\mu$m.

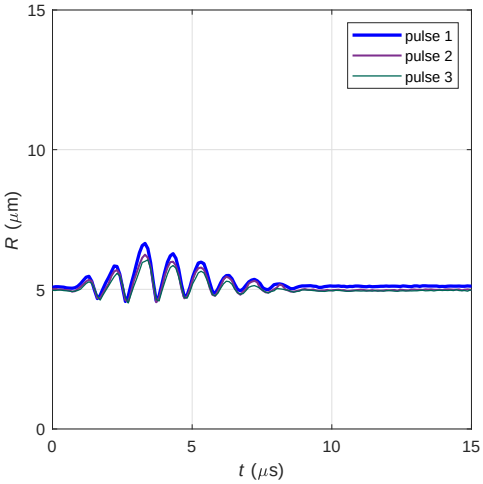

(d) $R_0 = 5.07\,\mu$m.

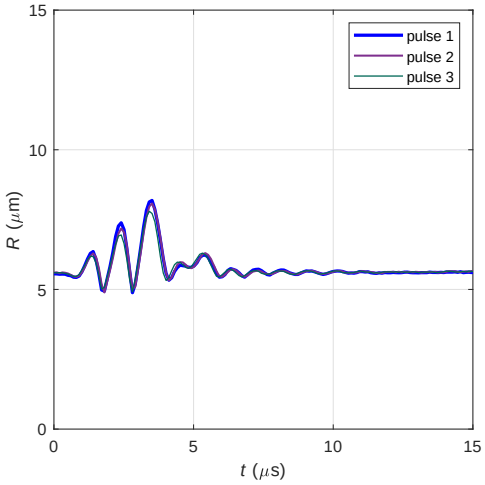

(e) $R_0 = 5.56\,\mu$m.

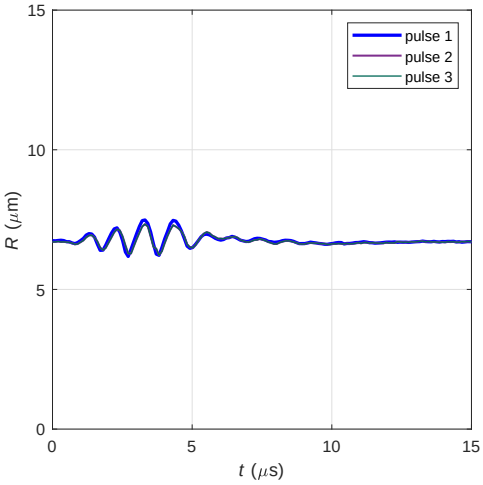

(f) $R_0 = 6.75\,\mu$m.

Figure 5.12: R(t) curves comparing the oscillatory response of individual AB1 antibubbles during exposure to multiple ultrasound pulses. The response owing to the first pulse is shown in blue, the response to the second pulse is shown in dark purple and the response to the third pulse is shown in bottle green. Each sub-figure illustrates the comparative oscillations for an antibubble with a different initial radius.

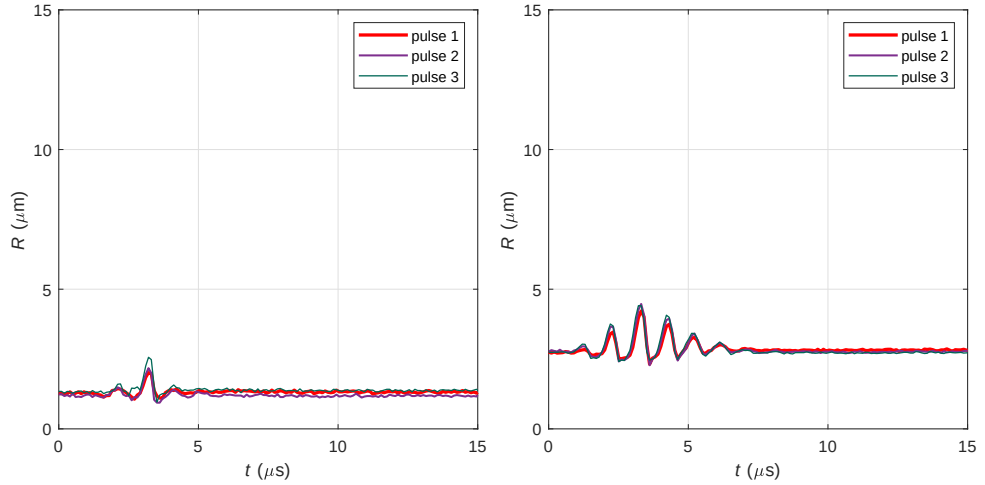

(a) $R_0 = 1.23\,\mu$m.

(b) $R_0 = 2.75\,\mu$m.

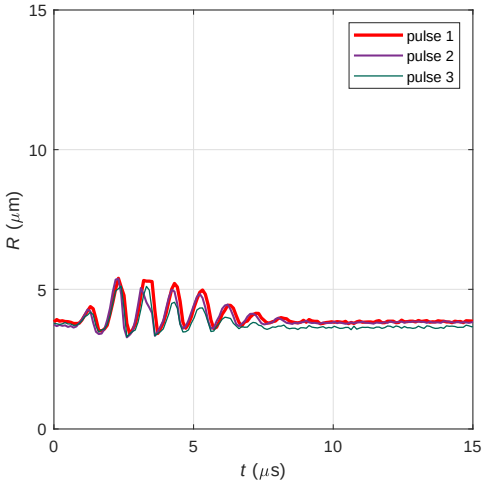

(c) $R_0 = 3.83\,\mu$m.

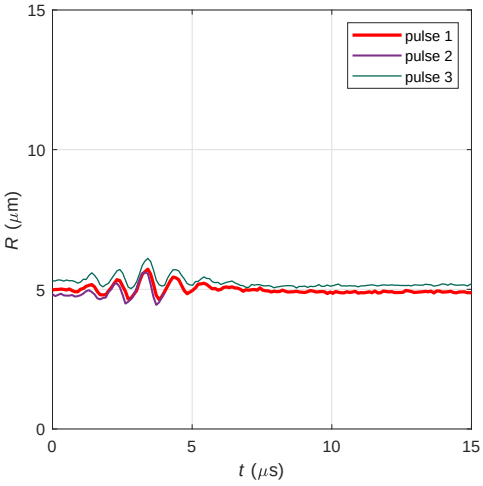

(d) $R_0 = 4.98\,\mu$m.

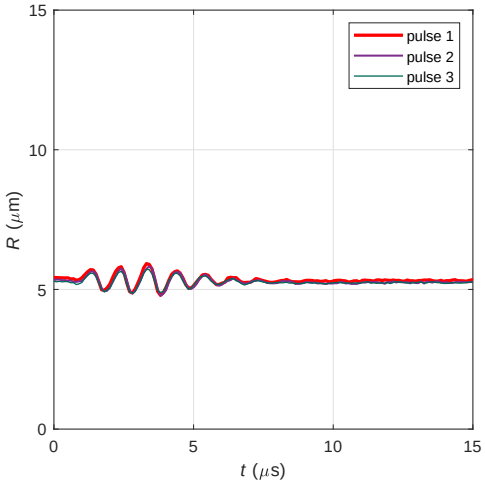

(e) $R_0 = 5.43\,\mu$m.

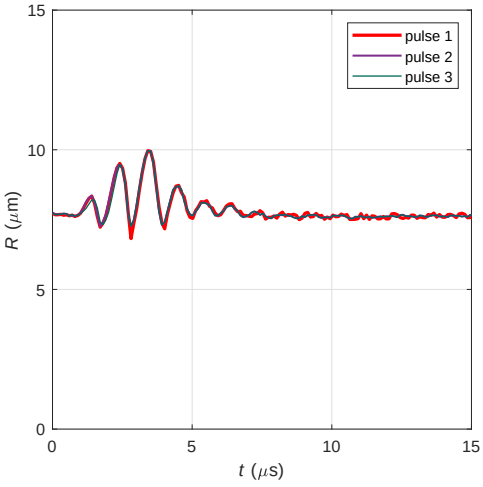

(f) $R_0 = 7.72\,\mu$m.

Figure 5.13: R(t) curves comparing the oscillatory response of individual AB2 antibubbles during exposure to multiple ultrasound pulses. The response owing to the first pulse is shown in red, the response to the second pulse is shown in dark purple and the response to the third pulse is shown in bottle green. Each sub-figure illustrates the comparative oscillations for an antibubble with a different initial radius.

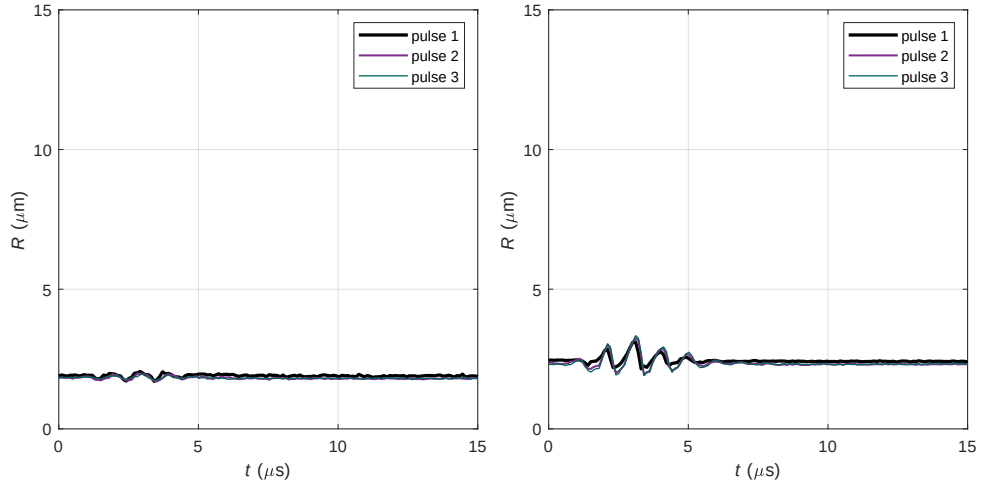

(a) $R_0 = 1.90\,\mu$m.

(b) $R_0 = 2.45\,\mu$m.

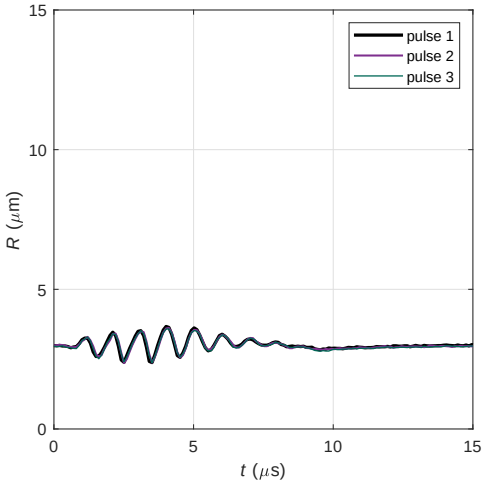

(c) $R_0 = 2.98\,\mu$m.

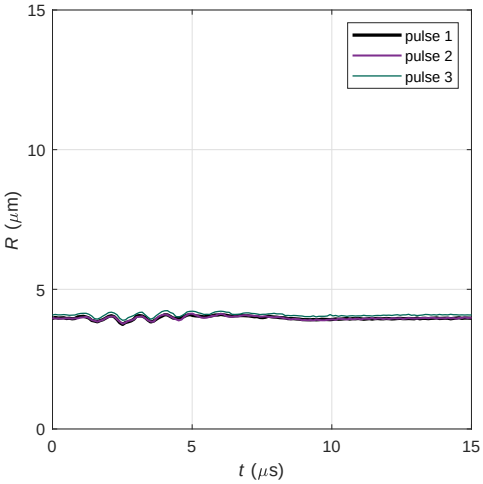

(d) $R_0 = 3.96\,\mu$m.

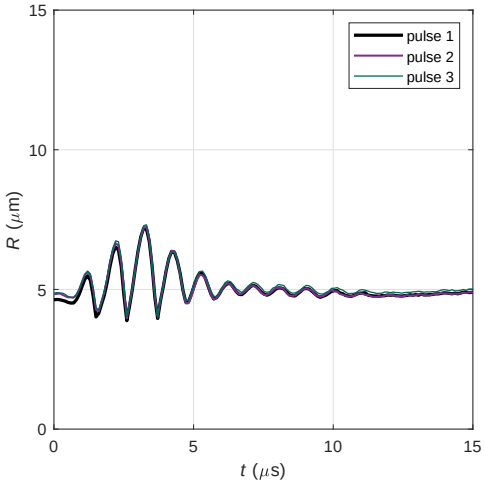

(e) $R_0 = 4.63\,\mu$m.

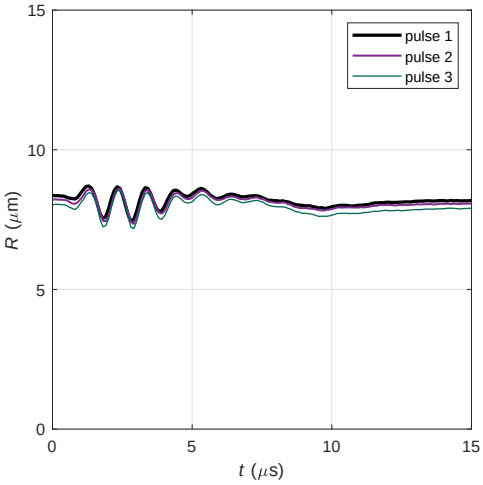

(f) $R_0 = 8.37\,\mu$m.

Figure 5.14: R(t) curves comparing the oscillatory response of individual REF bubbles during exposure to multiple ultrasound pulses. The response owing to the first pulse is shown in black, the response to the second pulse is shown in dark purple and the response to the third pulse is shown in bottle green. Each sub-figure illustrates the comparative oscillations for a bubble with a different initial radius.

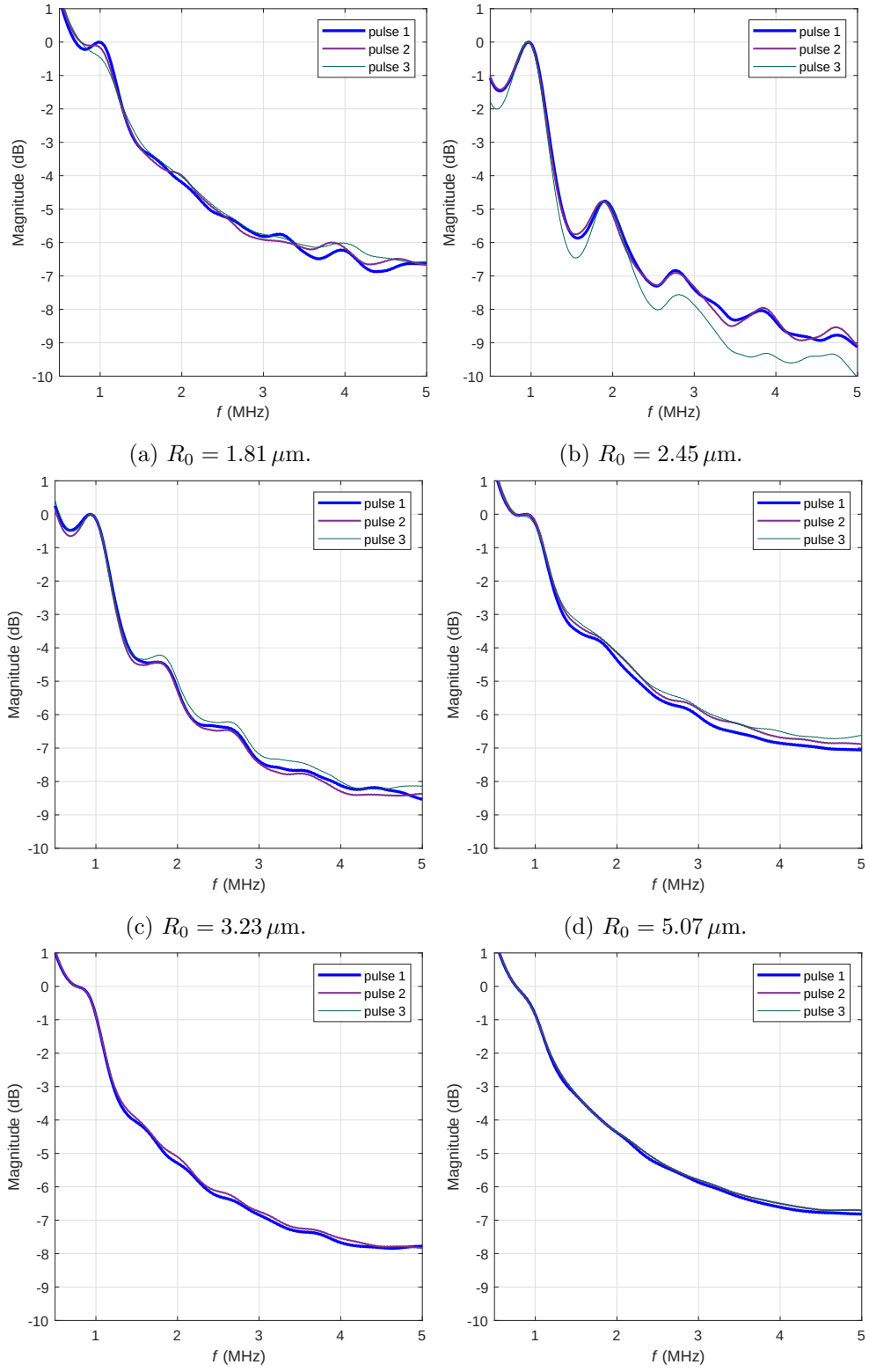

(a) $R_0 = 1.81\,\mu$m. (b) $R_0 = 2.45\,\mu$m.

(c) $R_0 = 3.23\,\mu$m. (d) $R_0 = 5.07\,\mu$m.

(e) $R_0 = 5.56\,\mu$m. (f) $R_0 = 6.75\,\mu$m.

Figure 5.15: FFTs comparing the frequency response of individual AB1 antibubbles during exposure to multiple ultrasound pulses. The response owing to the first pulse is shown in blue, the response to the second pulse is shown in dark purple and the response to the third pulse is shown in bottle green. Each sub-figure illustrates the comparative oscillations for an antibubble with a different initial radius.

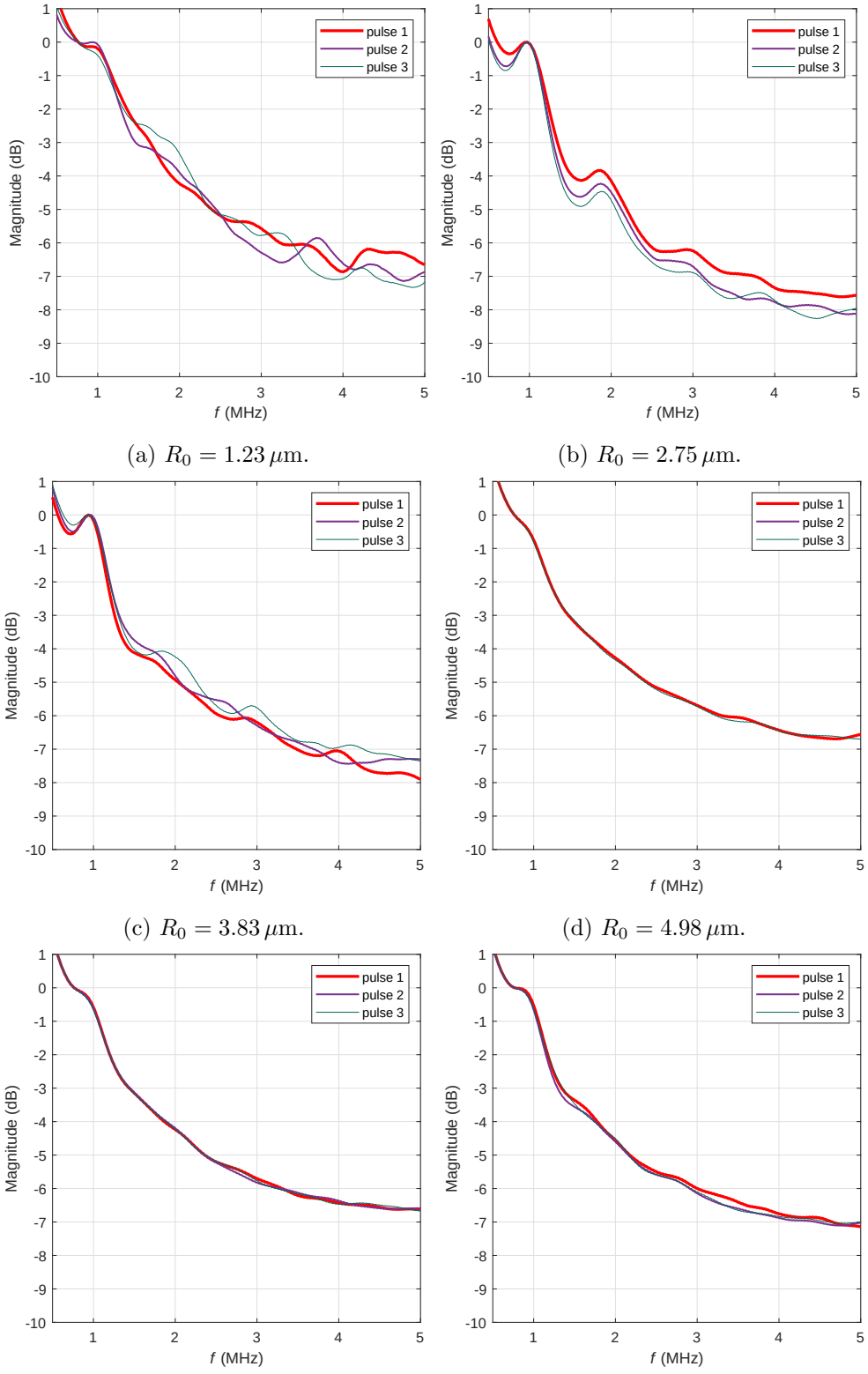

(a) $R_0 = 1.23\,\mu$m. (b) $R_0 = 2.75\,\mu$m.

(c) $R_0 = 3.83\,\mu$m. (d) $R_0 = 4.98\,\mu$m.

(e) $R_0 = 5.43\,\mu$m. (f) $R_0 = 7.72\,\mu$m.

Figure 5.16: FFTs comparing the frequency response of individual AB2 antibubbles during exposure to multiple ultrasound pulses. The response owing to the first pulse is shown in red, the response to the second pulse is shown in dark purple and the response to the third pulse is shown in bottle green. Each sub-figure illustrates the comparative oscillations for an antibubble with a different initial radius.

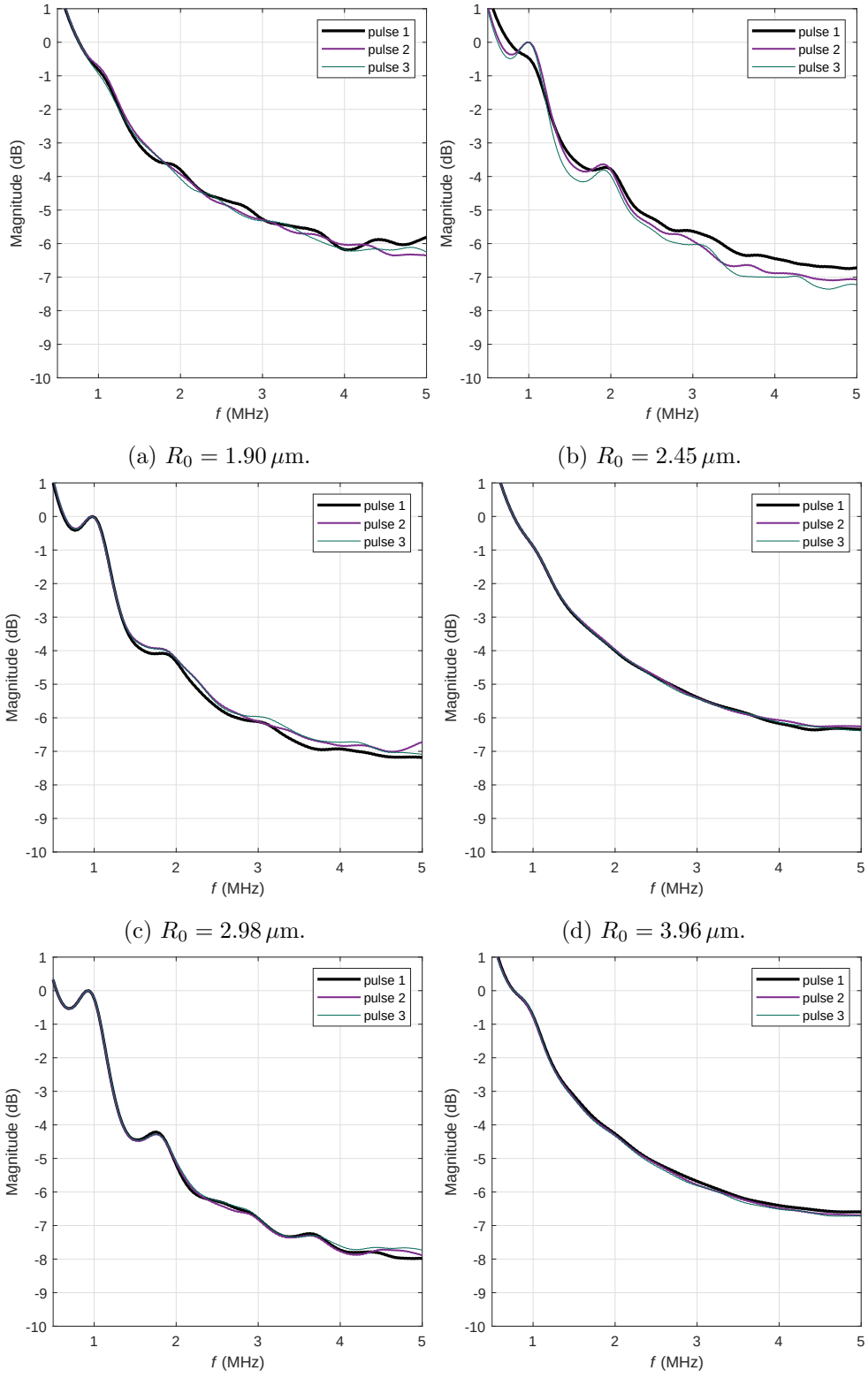

(a) $R_0 = 1.90\,\mu$m. (b) $R_0 = 2.45\,\mu$m.

(c) $R_0 = 2.98\,\mu$m. (d) $R_0 = 3.96\,\mu$m.

(e) $R_0 = 4.63\,\mu$m. (f) $R_0 = 8.37\,\mu$m.

Figure 5.17: FFTs comparing the frequency response of individual REF bubbles during exposure to multiple ultrasound pulses. The response owing to the first pulse is shown in black, the response to the second pulse is shown in dark purple and the response to the third pulse is shown in bottle green. Each sub-figure illustrates the comparative oscillations for a bubble with a different initial radius.

Prior exposure to ultrasound with amplitude 1 V showed no effect on either the time or frequency response for any of the (anti)bubble types.

5.4 Fragmentation

Fragmentation of antibubbles and bubbles is compared and discussed in this section. Figure 5.18 presents four selected frames from the footage of an AB1 antibubble sample exposed to ultrasound with an acoustic amplitude of 1 V next to four selected frames of an AB1 antibubble sample exposed to ultrasound with an acoustic amplitude of 5 V. Figures 5.19 and 5.20 show similar comparisons for AB2 antibubbles and REF bubbles respectively. The amount of positive excursion, negative excursion and overall oscillation asymmetry relative to the (anti)bubble equilibrium radii of the (anti)bubbles which met the criteria for image processing were compared for each (anti)bubble set under both ultrasound conditions. Tables 5.5 to 5.9 give the amount of positive excursion, negative excursion and overall oscillation asymmetry relative to (anti)bubble equilibrium radii for each of the (anti)bubble samples sets shown in Figures 5.18 to 5.20. This allows for the quantification of radii changes observed and a comparison to the expected values given in Tables 5.1 to 5.4.

Lastly, an unusual case of extreme positive excursion, following the fragmentation and subsequence coalescence of AB1 antibubbles during sonication, is presented in Figures 5.21 and 5.22.

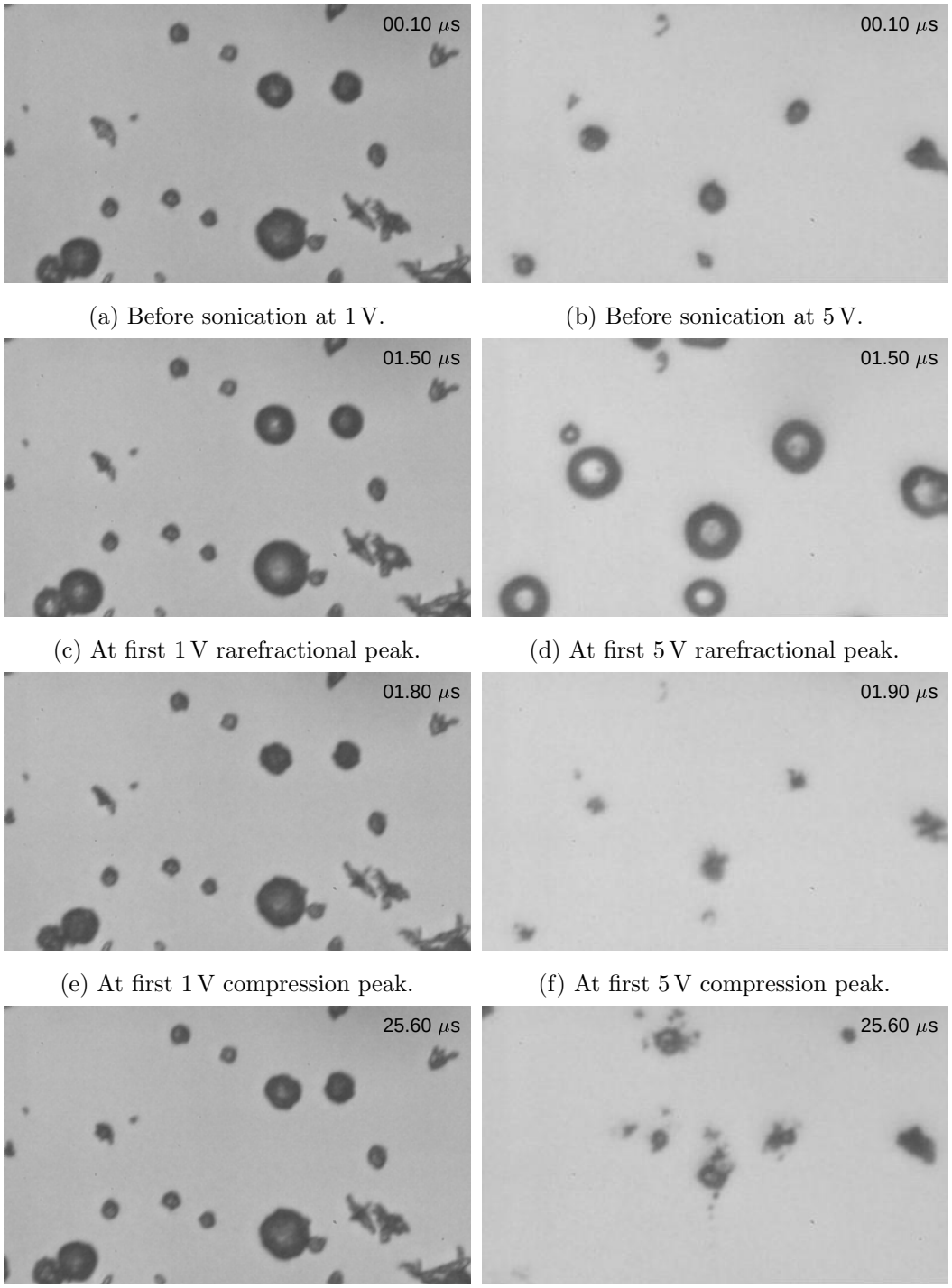

(a) Before sonication at 1 V.

(b) Before sonication at 5 V.

(c) At first 1 V rarefractional peak.

(d) At first 5 V rarefractional peak.

(e) At first 1 V compression peak.

(f) At first 5 V compression peak.

(g) After sonication at 1 V.

(h) After sonication at 5 V.

Figure 5.18: High-speed frames showing the impact of the amplitude of the applied ultrasound on AB1 antibubbles. The figures on the left show frames of AB1 antibubbles at different times during ultrasound exposure at an amplitude of 1 V, whilst the figures on the right show the comparative frames of AB1 antibubbles during ultrasound exposure at an amplitude of 5 V.

Table 5.5: AB1 antibubble positive excursion, negative excursion, oscillation asymmetry and the respective percentages thereof relative to equilibrium radii during exposure to ultrasound with a peak negative pressure of 200 kPa.

$R_0(\mu\mathbf{m})$	$\xi^+(\mu\mathbf{m})$	% **of** R_0	$\xi^-(\mu\mathbf{m})$	% **of** R_0	$\xi^+ - \xi^-(\mu\mathbf{m})$	% **of** R_0
1.76	0.035	2.01	0.060	3.44	-0.025	-1.43
2.29	0.063	2.76	0.171	7.48	-0.108	-4.72
2.47	0.059	2.37	0.060	2.43	-0.001	-0.06
2.66	0.055	2.05	0.096	3.62	-0.042	-1.57
2.71	0.194	7.17	0.102	3.79	0.092	3.39
2.99	0.184	6.15	0.136	4.56	0.047	1.58
2.99	0.055	1.85	0.092	3.08	-0.037	-1.23
3.20	0.239	7.48	0.154	4.81	0.085	2.67
3.28	0.094	2.88	0.051	1.57	0.043	1.31
3.41	0.144	4.23	0.138	4.04	0.006	0.19
3.75	0.153	4.08	0.647	17.26	-0.494	-13.18
4.94	0.457	9.26	0.528	10.69	-0.071	-1.43
5.56	0.797	14.33	0.622	11.18	0.175	3.15
Averages						
3.23	0.195	5.12	0.220	6.00	-0.025	-0.87

Table 5.6: AB1 antibubble positive excursion, negative excursion, oscillation asymmetry and the respective percentages thereof relative to equilibrium radii during exposure to ultrasound with a peak negative pressure of 1 MPa.

$R_0(\mu\mathbf{m})$	$\xi^+(\mu\mathbf{m})$	% **of** R_0	$\xi^-(\mu\mathbf{m})$	% **of** R_0	$\xi^+ - \xi^-(\mu\mathbf{m})$	% **of** R_0
1.65	1.940	117.68	0.626	37.98	1.314	79.70
2.12	4.271	201.86	0.872	41.20	3.399	160.67
3.42	4.376	127.88	1.504	43.94	2.873	83.94
4.36	5.217	119.79	1.459	33.51	3.758	86.29
4.42	4.060	91.76	1.518	34.30	2.542	57.46
4.70	4.222	89.93	0.666	14.20	3.556	75.73
Averages						
3.44	3.255	124.82	1.107	34.19	2.907	90.63

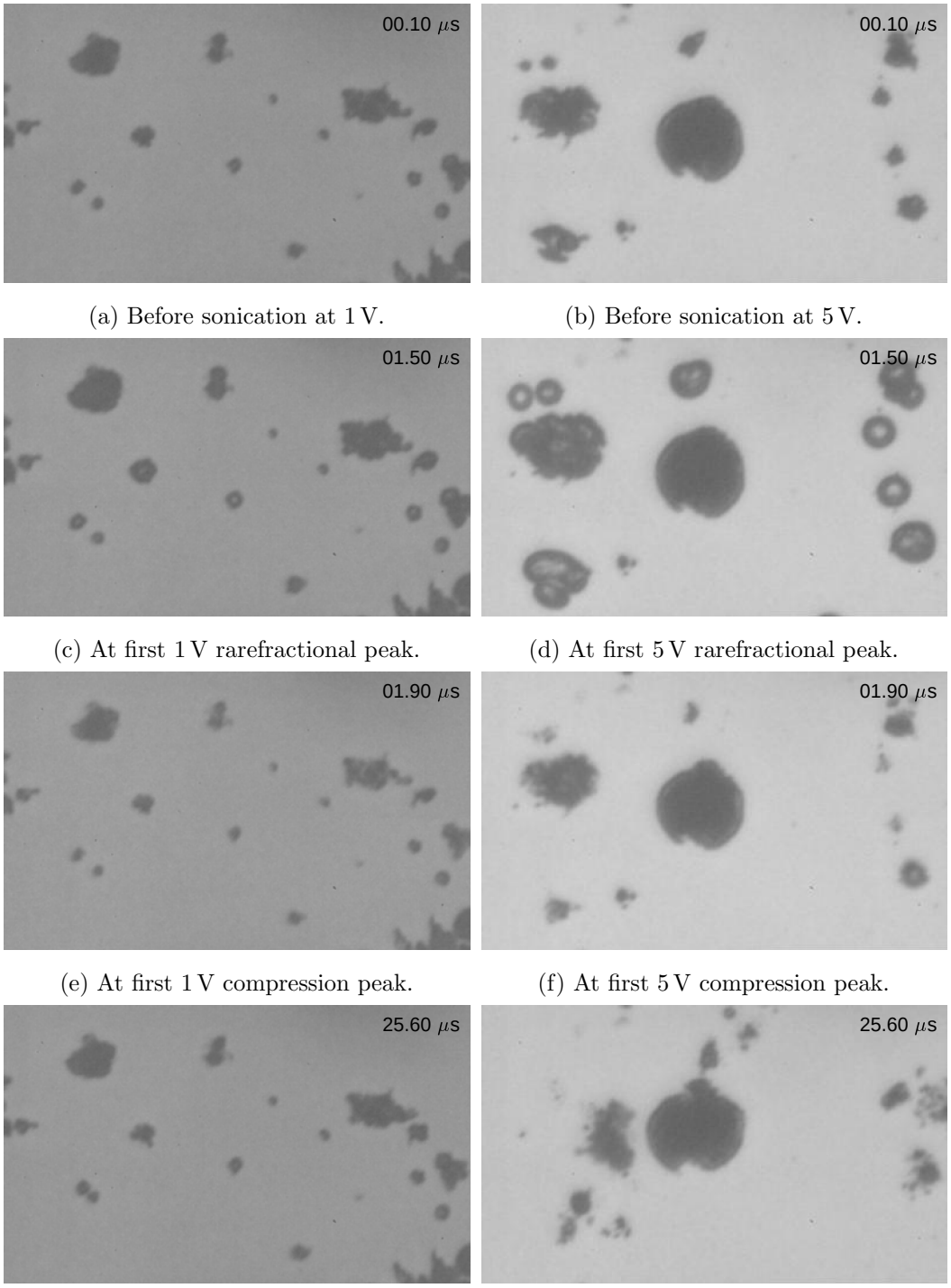

(a) Before sonication at 1 V.

(b) Before sonication at 5 V.

(c) At first 1 V rarefractional peak.

(d) At first 5 V rarefractional peak.

(e) At first 1 V compression peak.

(f) At first 5 V compression peak.

(g) After sonication at 1 V.

(h) After sonication at 5 V.

Figure 5.19: High-speed frames showing the impact of the amplitude of the applied ultrasound on AB2 antibubbles. The figures on the left show frames of AB2 antibubbles at different times during ultrasound exposure at an amplitude of 1 V, whilst the figures on the right show the comparative frames of AB2 antibubbles during ultrasound exposure at an amplitude of 5 V.

Table 5.7: AB2 antibubble positive excursion, negative excursion, oscillation asymmetry and the respective percentages thereof relative to equilibrium radii during exposure to ultrasound with a peak negative pressure of 200 kPa.

$R_0(\mu\mathbf{m})$	$\xi^+(\mu\mathbf{m})$	% **of** R_0	$\xi^-(\mu\mathbf{m})$	% **of** R_0	$\xi^+ - \xi^-(\mu\mathbf{m})$	% **of** R_0
1.92	0.207	10.78	0.257	13.40	-0.050	-2.62
2.26	0.447	19.77	0.214	9.46	0.233	10.30
2.35	0.514	21.85	0.284	12.10	0.229	9.76
2.39	0.226	9.48	0.230	9.66	-0.004	-0.18
2.51	0.058	2.31	0.085	3.39	-0.027	-1.08
2.65	0.376	14.17	0.171	6.46	0.205	7.72
3.14	0.323	10.28	0.279	8.87	0.044	1.41
3.47	0.610	17.61	0.290	8.36	0.320	9.25
3.84	0.443	11.55	0.415	10.81	0.028	0.74
6.79	0.802	11.81	0.512	7.54	0.290	4.28
7.20	0.753	10.46	0.635	8.82	0.118	1.64
Averages						
3.50	0.433	12.73	0.307	8.99	0.126	3.75

Table 5.8: AB2 antibubble positive excursion, negative excursion, oscillation asymmetry and the respective percentages thereof relative to equilibrium radii during exposure to ultrasound with a peak negative pressure of 1 MPa.

$R_0(\mu\mathbf{m})$	$\xi^+(\mu\mathbf{m})$	% **of** R_0	$\xi^-(\mu\mathbf{m})$	% **of** R_0	$\xi^+ - \xi^-(\mu\mathbf{m})$	% **of** R_0
1.77	0.689	38.90	0.399	22.54	0.290	16.36
2.06	0.696	33.86	0.332	16.16	0.364	17.71
2.45	0.052	2.11	0.052	2.11	0.000	0.00
2.77	1.100	39.66	0.295	10.62	0.806	29.04
3.03	0.978	32.24	0.282	9.30	0.696	22.95
3.58	1.371	38.27	0.435	12.14	0.936	26.13
4.43	1.100	24.83	0.592	13.37	0.508	11.46
6.46	2.328	36.08	0.214	3.32	2.114	32.76
9.32	2.994	32.12	1.311	14.06	1.683	18.06
13.24	0.385	2.90	0.284	2.15	0.100	0.76
Averages						
4.91	1.169	28.10	0.420	10.57	0.750	17.5

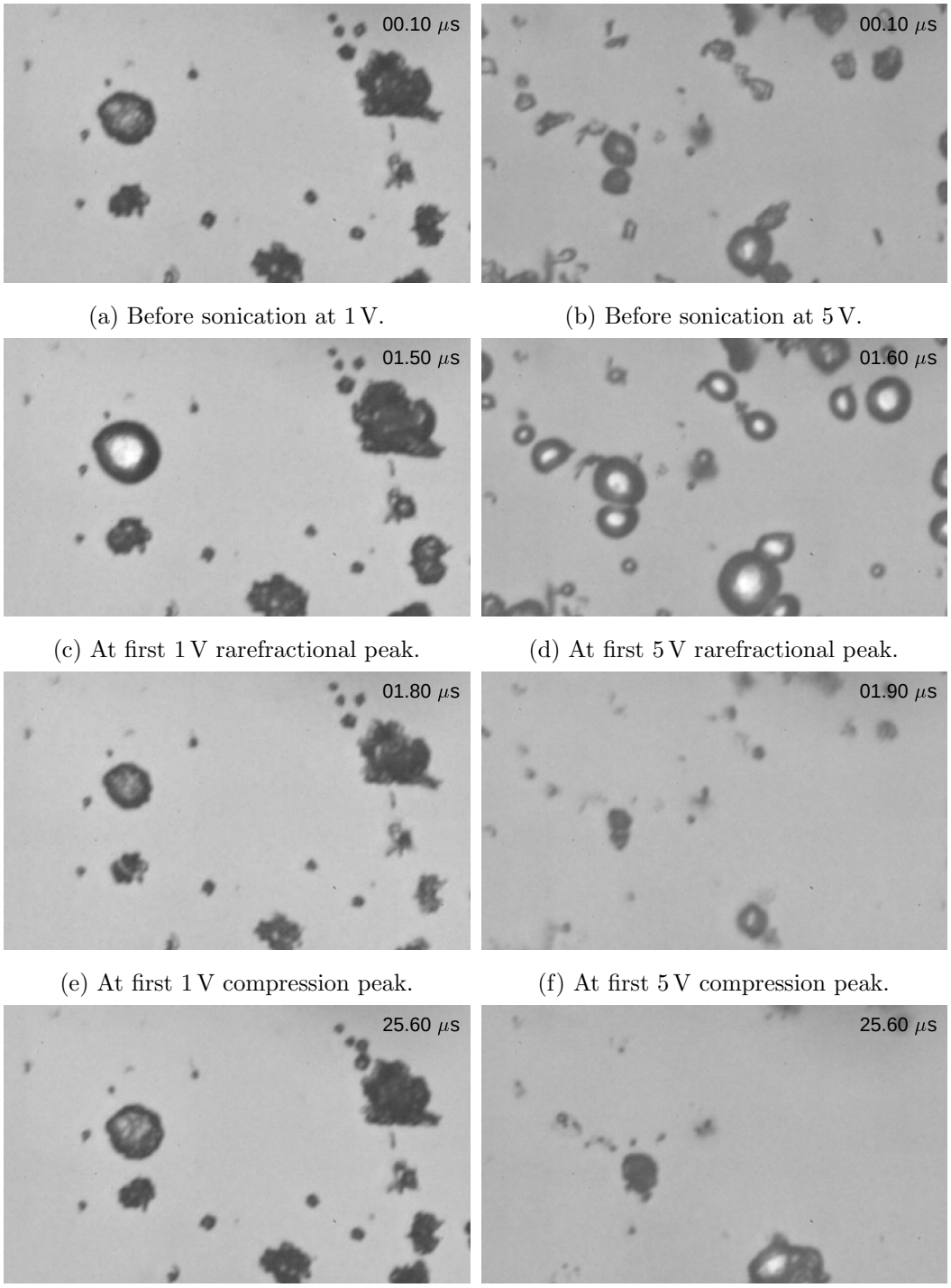

(a) Before sonication at 1 V.

(b) Before sonication at 5 V.

(c) At first 1 V rarefractional peak.

(d) At first 5 V rarefractional peak.

(e) At first 1 V compression peak.

(f) At first 5 V compression peak.

(g) After sonication at 1 V.

(h) After sonication at 5 V.

Figure 5.20: High-speed frames showing the impact of the amplitude of the applied ultrasound on REF bubbles. The figures on the left show frames of REF bubbles at different times during ultrasound exposure at an amplitude of 1 V, whilst the figures on the right show the comparative frames of REF bubbles during ultrasound exposure at an amplitude of 5 V.

Table 5.9: Reference bubble positive excursion, negative excursion, oscillation asymmetry and the respective percentages thereof relative to equilibrium radii during exposure to ultrasound with a peak negative pressure of 200 kPa.

$R_0(\mu\mathbf{m})$	$\xi^+(\mu\mathbf{m})$	**% of** R_0	$\xi^-(\mu\mathbf{m})$	**% of** R_0	$\xi^+ - \xi^-(\mu\mathbf{m})$	**% of** R_0
1.65	0.226	13.68	0.456	27.68	-0.231	-14.00
1.69	0.085	5.02	0.212	12.55	-0.127	-7.53
1.95	0.778	39.86	0.448	22.97	0.330	16.89
2.13	0.541	25.46	0.319	15.02	0.222	10.45
2.24	0.465	20.76	0.617	27.54	-0.152	-6.78
2.26	0.431	19.08	0.276	12.22	0.155	6.86
2.49	0.822	33.05	0.248	9.95	0.575	23.10
2.50	0.692	27.71	0.493	19.73	0.199	7.97
5.44	1.109	20.38	0.637	11.70	0.472	8.68
5.61	1.078	19.20	0.653	11.63	0.425	7.57
7.24	1.390	19.20	1.020	14.09	0.370	5.11
8.58	1.652	19.24	1.260	14.68	0.392	4.57
10.94	1.362	12.45	1.063	9.72	0.299	2.74
Averages						
4.21	0.818	21.16	0.592	16.11	0.225	5.05

Table 5.10: Reference bubble positive excursion, negative excursion, oscillation asymmetry and the respective percentages thereof relative to equilibrium radii during exposure to ultrasound with a peak negative pressure of 1 MPa.

$R_0(\mu\mathbf{m})$	$\xi^+(\mu\mathbf{m})$	% **of** R_0	$\xi^-(\mu\mathbf{m})$	% **of** R_0	$\xi^+ - \xi^-(\mu\mathbf{m})$	% **of** R_0
1.92	0.873	45.49	1.051	54.77	-0.178	-9.29
2.20	0.019	0.86	0.686	31.14	-0.667	-30.28
2.60	1.747	67.11	0.904	34.74	0.843	32.37
2.80	0.849	30.26	1.703	60.72	-0.854	-30.46
3.10	1.255	40.55	1.266	40.89	-0.011	-0.34
3.25	0.083	2.55	1.151	35.45	-1.068	-32.90
3.63	1.813	50.00	1.632	45.01	0.181	4.99
3.95	1.111	28.16	2.132	54.05	-1.021	-25.89
4.09	1.501	36.74	1.086	26.59	0.414	10.14
4.11	1.984	48.26	1.797	43.71	0.187	4.55
4.42	1.414	31.97	2.465	55.74	-1.051	-23.77
4.81	1.730	36.00	2.086	43.42	-0.356	-7.42
4.97	1.196	24.09	2.356	47.45	-1.160	-23.36
5.11	2.169	42.50	2.526	49.48	-0.357	-6.99
6.14	2.001	32.59	2.695	43.90	-0.694	-11.31
7.07	2.828	40.00	2.719	38.46	0.109	1.54
Averages						
4.01	1.411	34.82	1.766	44.10	-0.355	-9.28

While all samples show clear fragmentation after the first compression peak when sonicated at 5 V, it appears that the amount of dispersion of the fragments decreases with an increase in the amount of endoskeletal content present.

An unusual case of extreme positive excursion, following the fragmentation and subsequence coalescence of AB1 antibubbles during sonication, is presented in Figures 5.21 and 5.22. While fragmentation occurred during each compression cycle, the AB1 antibubble fragments coalesced with other nearby AB1 antibubble fragments and began to expand a full 10 μs after the last cycle of ultrasound was applied. The coalesced antibubble grew to 39.52 μm in size, 9 μm larger than during sonication. There were similar instances in which coalesced antibubbles showed extreme positive excursion after sonication, but neither surpassed the maximum size during sonication.

This behaviour was not observed in the reference bubble footage.

(Anti)bubbles that had undergone fragmentation, and split into a number of smaller (anti)bubbles and re-coalesced were not considered in investigation of the first two objectives. This is because as entirely different (anti)bubbles, their oscillation could not be compared against the initial (anti)bubble's equilibrium radii. Figure 5.22 shows the radius(time) curve of an antibubble that has undergone both fragmentation and coalescence multiple times and is thus not the same antibubble throughout. The antibubble fragments would only be visible for a single frame in which, for the radius(time) curve, they were measured as if they were just one antibubble.

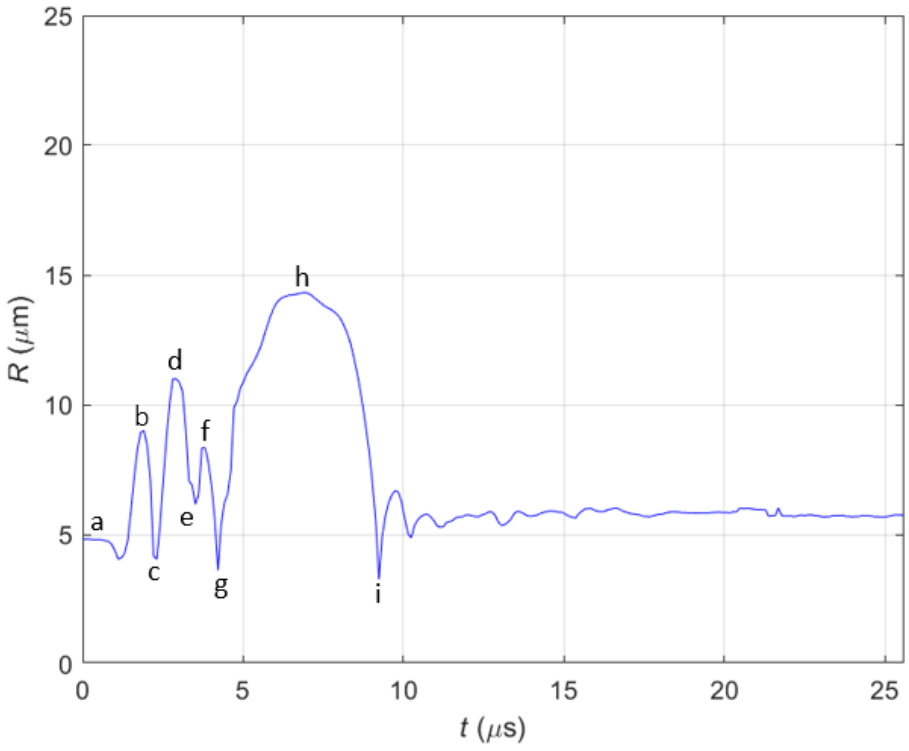

Figure 5.21: Antibubble positive excursion behaviour through fragmentation and coalescence whilst under sonication at 5 V.

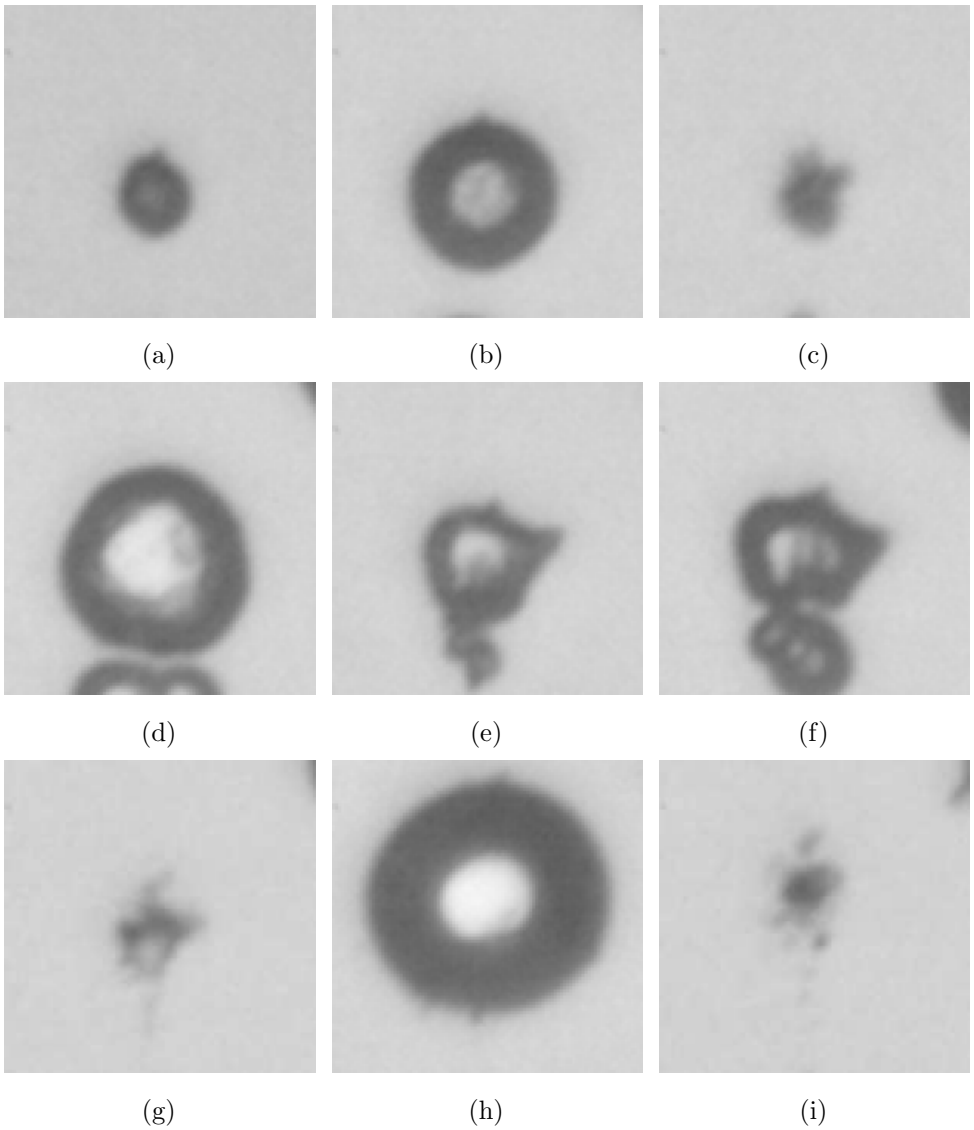

Figure 5.22: Fragmentation and coalescence of an AB1 antibubble sample whilst under sonication as 5 V. Prior to sonication a single antibubble (a) is observed, predictably it reaches maximum positive excursion during the first cycle of ultrasound (b) and subsequently fragments (c) at maximum negative excursion during the same ultrasound cycle. Subfigure (d) shows the maximum positive excursion of coalesced fragments during second cycle, (e) the approach of surrounding antibubbles during the subsequent compression phase, (f) antibubble positive excursion during the third cycle and (g) fragmentation at maximum negative excursion during the third ultrasound cycle. The unusual positive excursion behaviour after sonication is shown in the final two subfigures where, (h) shows the maximum positive excursion of the coalesced antibubble and (i) shows the final antibubble fragments after sonication.

Chapter 6

Discussion

6.1 To objective 1: expansion-only hypothesis

The expansion-only hypothesis of antibubbles assumes that the liquid core of an antibubble is incompressible and thus does not allow for antibubble negative excursion beyond it's droplet core size. To investigate this hypothesis; and the role that the amplitude of the applied ultrasound had on both AB1 antibubbles and REF bubbles were compared at both 1 V (PNP of 200 kPa) and 5 V (PNP of 1 MPa).

Figure 5.2 shows the amount of positive excursion (anti)bubbles experience during the first cycle of exposure to two different acoustic amplitudes. In Figure 5.2a, in which the results for exposure an amplitude of 1 V are shown, the reference bubbles appear to have undergone marginally greater positive excursion than the antibubbles did. The linear regression polynomial (5.1) of antibubbles under sonication at a peak acoustic amplitude of 1 V, as well as the expected average positive excursion relative to equilibrium radii of 5.67% given in Table 5.1, indicate that limited positive excursion occurred. The linear regression polynomial (5.3) of the reference bubbles under sonication at 1 V, coupled with the expected average positive excursion relative to initial radii of 13.32% shown in Table 5.2, indicate that reference bubble positive excursion is expected to be more than double that of antibubble positive excursion under the same acoustic conditions. Theoretically (3.3) indicates that antibubbles should expand more than reference bubbles owing to the additional internal pressure caused by the liquid droplet core [1]. This was not the case under this low amplitude acoustic regime. This may be the result of antibubbles having a higher resonant frequency than bubbles of equal outer diameter although, a more likely explanation would be that the presence of an enoskeleton hampers antibubble oscillation.

After exposure to a single 1 MHz ultrasound cycle at 5 V, Figure 5.2b illustrates that both reference bubbles and antibubbles exhibit substantial positive excursion. Linear regression polynomials (5.5) and (5.7) as well as the respective average positive excursion per (anti)bubble type relative to equilibrium radii size of 80.59% and 53.08%, shown in Tables 5.3 and 5.4, show that antibubbles undergo greater positive excursion than reference bubbles do at high acoustic amplitudes. This is in line

with [1, 39] and the Rayleigh-Plesset equation of antibubble dynamics (3.3) which suggest that antibubbles expand more relative to their equilibrium radius than reference bubbles do.

Tables 5.1 and 5.3 indicate that when exposed to a 1 MHz ultrasound pulse, the amount of positive excursion experienced by an antibubble relative to the initial radii is expected to lessen with increasing equilibrium antibubble size. The same phenomena can be observed for reference bubbles in Tables 5.2 and 5.4.

Figure 5.4a suggests that exposure to an ultrasound pulse with an amplitude of 1 V results in less negative excursion of antibubbles than reference bubbles. Linear regression polynomials (5.9) and (5.11) indicate limited negative excursion for both types of (anti)bubbles under this acoustic regime. Tables 5.1 and 5.2 show that, on average, antibubbles are expected to contract by nearly half the amount (7.05%) that reference bubbles do (15.31%) relative to their equilibrium size. The amount of negative excursion experienced under this low amplitude acoustic regime is expected to increase with equilibrium (anti)bubble size.

Clear negative excursion for both antibubbles and bubbles is shown in Figure 5.4b, with regression lines (5.13) and (5.15) confirming this. It is evident that whilst under exposure to a high amplitude ultrasonic regime, reference bubbles contract more than antibubbles do. Tables 5.3 and 5.4 indicate that antibubbles are expected to contract by about 25% of their equilibrium size, whilst reference bubbles have a comparative expected average negative excursion of 41.92%. The reduced negative excursion in antibubbles can be attributed to their incompressible core, which serves to confirm the expansion-only hypothesis. In contrast to their expected negative excursion behaviour at 1 V, Tables 5.1 and 5.2 indicate that percentage negative excursion relative to the equilibrium radii of (anti)bubbles exposed to 5 V should decrease with increasing equilibrium (anti)bubble size.

The oscillation asymmetry of antibubbles and bubbles as a result of a single cycle of ultrasound is compared in Figure 5.6. Figure 5.6a shows that both antibubbles and bubbles oscillate symmetrically whilst exposed to an ultrasound pulse with a peak negative pressure of 200 kPa. Both the antibubble and reference bubble 1 V linear regression polynomials (5.17) and (5.18) indicate negligible asymmetry. This is further confirmed in Tables 5.1 and 5.2, as a minute average oscillate symmetrically of only -1.38% for antibubbles and -2.07% for reference bubbles is observed.

In Figure 5.6b it is clear that AB1 antibubbles experience significantly higher oscillation asymmetry than reference bubbles do. Antibubbles also present a more

asymmetric oscillatory response at this higher acoustic amplitude, with Table 5.4 showing an average expected positive oscillation asymmetry of 55.01%. Table 5.4 shows that for reference bubbles equal to or below 6 μm in size, positive excursion is greater than negative excursion, despite the linear regression polynomial for reference bubbles oscillation asymmetry (5.20) having a negative slope. The percentage of expected overall oscillation asymmetry only becomes negative for reference bubbles that have an equilibrium radius larger than 6 μm in size and the overall average oscillation asymmetry for bubbles between 2 μm to 10 μm is still expected to be positive 11.04%.

It can be observed that increasing the driving amplitude of the applied ultrasound resulted in increased asymmetric radial excursion for both reference bubbles and antibubbles. This confirms that increasing the acoustic amplitude of the applied ultrasound, increases (anti)bubble oscillation asymmetry as suggested by [26] and (3.3). Table 5.1 indicates that when exposed to a low amplitude acoustic regime, antibubble oscillation asymmetry is expected to become more asymmetric, with greater negative excursion being observed as equilibrium size is increased. The increased amount of negative excursion for larger antibubbles is probably a result of the ratio of outer antibubble diameter to inner droplet core diameter increasing as antibubble equilibrium size grows larger. When exposed to a high amplitude acoustic regime, Tables 5.3 and 5.4 show a decrease in positive oscillation asymmetry with increasing (anti)bubble size, this is probably also a result of the increased ratio of outer radii to inner core radii allowing for more space to contract.

Ultimately these results confirm the expansion-only hypothesis for antibubbles under high acoustic amplitude regimes, as their oscillation asymmetry is highly positively skewed whilst reference bubble oscillation asymmetry is considerable more symmetric.

6.2 To objective 2: endoskeletal effect on oscillation reliability and stability

The investigation into the oscillatory response of antibubbles under ultrasound with a peak negative pressure of 200 kPa indicated that antibubbles behaved more reliably and stably than microbubbles. (Anti)bubbles that had been exposed to a driving amplitude of 5 V were not included in the investigation as (anti)bubble fragmentation and coalescence occurred frequently, making it impossible to relate the final fragments to the initial (anti)bubbles they were once a part of.

Figure 5.7 shows the change in bubble and antibubble radii owing to exposure to a full ultrasound pulse, consisting of thee cycles, with a driving amplitude of 1 V. The linear polynomial function for AB1 at 1 V (5.21) indicates a negligible change in equilibrium radius. When exposed to the same ultrasonic conditions the linear regression curve of the reference bubbles (5.22) describes an approximate radii shrinkage of 0.15 μm after sonication. The endoskeletal content of antibubbles appears to assist in maintaining the equilibrium radius, even after sonication. This could mean that antibubbles could be exposed to low amplitude ultrasound for longer periods of time, making reliable high precision targeted drug delivery a possibility. The lower lasting impact experienced by antibubbles compared to reference bubbles can probably be attributed to the significantly smaller amount of positive excursion experienced by antibubbles under the low amplitude ultrasound regime noted in the discussion of the expansion-only hypothesis.

The radius(time) curves comparing (anti)bubbles of the same type with similar initial radii presented in Figure 5.8, indicate that antibubbles are more reliable than reference bubbles. The reference bubbles in Figures 5.8e and 5.8f vary in oscillation amplitude far more than the AB1 antibubbles in Figures 5.8a and 5.8b do, whilst antibubbles of type AB2 appeared to show the least variation in oscillation in Figures 5.8c and 5.8d.

From Figure 5.9 it can be observed that the antibubble with the highest endoskeletal content, AB2, had the lowest oscillatory response in most cases, whilst reference bubbles, which contained no endoskeletal content, often exhibited the highest oscillatory response. Tables 5.1 and 5.2 support these results as antibubbles are expected to expand by an average of only 5.67% and contract by an average of 7.05% while reference bubbles are expected to expand by 13.32% and contract by 15.31%. The reference bubbles also appeared to exhibit the most varied oscillatory response for each of the radii ranges in Figure 5.9. This confirms that antibubbles are more stable than reference bubbles at low acoustic amplitudes. The increased stability and reduced oscillation observed in antibubbles is hypothesised to be a result of the presence of endoskeletal content within antibubbles.

Additionally the oscillation of antibubbles after sonication appear to grow faint within 3 μs after the application of the ultrasound pulse, whereas the reference bubble oscillations only appear to fade after approximately 10 μs. The comparably prolonged oscillation of the reference bubbles after sonication seen in Figure 5.9 indicates that the endoskeletal content of antibubbles may have damping properties. The frequency transforms corresponding to these (anti)bubble radius-time curves,

shown in Figures 5.10 and 5.11, suggest no significant harmonic differences exist between any of the (anti)bubbles across different equilibrium sizes. This indicates that both the size of the radius and the amount of endoskeletal content do not have a harmonic effect in the frequency domain.

Figures 5.12, 5.13 and 5.14 compare the oscillation of (anti)bubbles during exposure to a single low amplitude pulse of ultrasound to their oscillation during exposure to a second and third identical pulse. Prior exposure to sonication at a low acoustic amplitude appears to have no noticeable impact on the oscillation of any of the antibubble types, making them all similarly stable at low acoustic amplitudes. The frequency response comparison that was carried out on the same (anti)bubbles, shown in Figures 5.15, 5.16 and 5.17, presents no obvious change in the frequency domain. This indicates that prior exposure at 200 kPa negative pressure has no affect on the frequency response of any of the (anti)bubble types. If repeated sonication was applied with less wait-time between each pulse, a more noticeable effect could be observed.

The frequency response comparisons of antibubbles and bubbles of the same size under low amplitude sonication, shown in Figures 5.10, 5.11, suggest no significant harmonic differences exist between any of the (anti)bubbles across different equilibrium radii. Figures 5.15, 5.16 and 5.17 suggest that exposure to multiple ultrasound pulses does not alter this. In general the harmonics of the (anti)bubbles appear to be weaker for (anti)bubbles with initial radii greater than 2.5 μm. The relationship of decreasing linear resonance frequency with increase initial radius is in line with equation 3.4.

6.3 To objective 3: fragmentation

The investigation to determine whether antibubbles and bubbles would undergo fragmentation under the same ultrasonic conditions was completed successfully. Figures 5.18 to 5.20 show that a single, high-amplitude pulse, with a peak negative pressure of 1 MPa, was enough to shatter all (anti)bubble types. Cavitation is clearly observed in each of the (anti)bubbles exposed to ultrasound with an amplitude of 5 V, as the (anti)bubbles expanded to well above their equilibrium sizes during the first rarefaction peak, after which rapid collapse results in fragmentation. Surface instabilities can also be observed at the 5 V rarefactional peak for each to the (anti)bubble types.

All 90 of the measurable (anti)bubbles fragmented within a single cycle of sonication at

1 MHz with a peak negative pressure of 1 MPa. This indicates that all (anti)bubbles with initial radii greater than 1.65 μm should fragment within a single cycle of sonication at 1 MHz with peak negative pressure 1 MPa. No fragmentation was observed in the 243 (anti)bubbles that were exposed to ultrasound with a peak negative pressure of 200 kPa.

A comparison of the dispersion of (anti)bubble fragments seen in Figures 5.18, 5.19 and 5.20, suggests that dispersion of (anti)bubble fragments decreases with increasing endoskeletal content. AB2 antibubble fragments appear to disperse the least whilst reference bubble fragments appear to disperse the most. This could be a result of the hydrophobic properties of the endoskeletal content within the antibubbles. By clustering together the hydrophobic particles limit the surface area exposed to the surrounding water.

Tables 5.5 to 5.9 give the amount of positive excursion, negative excursion, oscillation asymmetry and the percentage thereof, relative to (anti)bubble equilibrium radii for each of the (anti)bubble samples sets shown in Figures 5.18 to 5.20. This allowed for the quantification of the changes observed and a comparison to the expected values given in Tables 5.1 to 5.4.

Table 5.5 shows that on average the percentage of positive excursion, negative excursion and oscillation asymmetry relative to the equilibrium (anti)bubble radii experienced by antibubbles of type AB1 differ from the expected averages given in Table 5.1 by no more than 1.4%. The average positive excursion of the antibubbles exposed to ultrasound with an amplitude of 5 V, shown in Table 5.6, differed from the expected average positive excursion seen in Table 5.6 by a large margin. This may be, in part, owing to the small sample size, a smaller average radius size and the linear regression line for oscillation asymmetry (5.19) being a non-ideal fit for the data. The lowest positive excursion percentage relative to radius size observed was 89.93% whilst under sonication at a peak acoustic amplitude of 5 V, indicating that cavitation was indeed the mechanism for fragmentation, with Blake's radius (3.9) being surpassed in most cases.

Tables 5.7 and 5.8 show that AB2 antibubble should expand more than they contract under both acoustic regimes. The additional endoskeletal content appeared to result in reduced radii negative excursion and positive excursion during oscillation. The total average oscillation asymmetry was also shown to be more symmetric for antibubbles of type AB2 than of type AB1. This lack of extreme oscillation contributes greatly to the observed high stability and predictability of AB2 antibubbles and further supports

the theory given in the expansion-only hypothesis discussion that the presence of an endoskeleton hampers antibubble oscillation at low amplitudes.

Tables 5.9 and 5.10 presented higher average oscillation asymmetry than the expected ones given in Tables 5.2 and 5.4, This could be attributed to a large portion of the samples having radii below $3\,\mu$m in size in Table 5.9 and less than $5\,\mu$m in Table 5.10 in size. The results confirm, once again, that references bubbles oscillate more symmetrically than antibubbles under sonication at a high acoustic amplitudes.

The extreme positive excursion after sonication illustrated in the radius vs time curve of Figure 5.21 and shown in Figure 5.22 could potentially be attributed to the phenomena described by (3.7) which indicates that (anti)bubble fragments contain more surface energy than the original (anti)bubble prior to sonication. The positive excursion of the coalesced new bubble took place more than $9\,\mu$s after sonication, indicating that a form of energy storage may have occurred.

6.4 Considerations for future work

An even distribution of experimental footage would make for more precise comparisons and analysis. Figure 5.1 shows the distributions of reference bubbles and antibubbles of type AB1 and AB2 that could be processed for this research. Ideally the distribution of (anti)bubbles would have been even across both sample type and size. This would have allowed for more comparison of antibubbles of the same size and more exact regression lines. More data on the effect of a high amplitude ultrasound pulse on sonication could also help to increase the accuracy of the regression lines produced. The influence of different control variables and experimental conditions on antibubble oscillation asymmetry should also be considered for future instigation.

An investigation into ultrasonic antibubble manipulation in terms of translation was out of the scope of this research but is visible in Figures 5.18 and 5.19, and would be integral in accessing their potential as ultrasound chemotherapeutic drug carriers. For this a comparison of the amount of translation experience per ultrasound pulse for antibubbles and bubbles under low amplitude sonication is required. Further investigation into the stage "energy storage" phenomena observed in some of the videos of antibubbles exposed to ultrasound with a peak negative pressure of 1 MPa could also yield some interesting results that may be of use for alternative applications.

Antibubbles with cores containing chemotherapeutics should be investigated under

ultrasound to determine whether the addition of chemotherapeutic material has as significant impact on the acoustic properties of antibubbles that have been observed in this study.

Chapter 7

Conclusion

Presently, there is no way to safely and reliably transport highly toxic chemicals such as chemotherapeutics through the body and then release them at a targeted site. The use of antibubbles as drug carriers may allow this to become a reality however, as it is believed that antibubbles possess acoustic properties that may be ideally suited to this purpose. The aim of this research was to investigate these acoustic properties through the completion of three objectives. The first of which, was to investigate the expansion-only hypothesis of antibubbles. This hypothesis suggests that the internal droplet cores of antibubbles hampers antibubble negative excursion when under sonication, ultimately resulting in highly asymmetric oscillation. The second objective involved investigating the reliability and stability of antibubbles by comparing the oscillation experienced whilst under sonication of antibubbles with different amounts of endoskeletal content that were similar in size. The effect of multiple ultrasonic pulses on these antibubbles was also investigated. The final objective was to determine whether antibubbles could be fragmented at the same acoustic amplitude at which microbubbles experience fragmentation.

To investigate these objectives, experimental footage of the sonication of antibubbles with different amounts of endoskeletal content was analysed. AB1 antibubbles contained liquid cores of 2 vol% endoskeletal content, AB2 antibubbles contained liquid cores of 10 vol% endoskeletal content and REF bubbles contained no liquid cores, and therefore no endoskeletal content. Image processing techniques were used to identify and quantify changes in individual antibubble radius sizes throughout sonication. The 1 MHz sonication was carried out at a low acoustic amplitude of 200 kPa and high acoustic amplitude of 1 MPa. Image processing techniques were used to identify and quantify changes in individual antibubble radius sizes throughout sonication. Analysis and comparison then followed.

The expansion-only hypothesis was confirmed for antibubbles exposed to high amplitude ultrasound with a transmitting frequency of 1 MHz. Antibubble oscillation was found to be more asymmetric than that of microbubbles under this acoustic regime, as the liquid droplet core of the antibubbles hampered antibubble negative excursion and increased the pressure within the antibubble, resulting in additional positive excursion.

Antibubbles were found to be more reliable and stable under the influence of ultrasound than microbubbles. Additionally a single pulse of ultrasound, with a peak negative pressure of 1 MPa, was shown to be enough to shatter antibubbles and bubbles alike, although the addition of endoskeletal content did lessen the dispersion of the internal contents.

The increased stability of antibubbles at low acoustic amplitudes indicates that they can be carefully controlled and used in diagnostics, whilst at higher acoustic amplitudes they can be made to rupture and release their contents. This makes them promising potential delivery agents for highly toxic chemicals such as chemotherapeutics. Ultrasound of a low amplitude could potentially be used reliably to manipulate antibubbles through the blood stream, towards the cancerous region of the body and a high amplitude pulse could be used to fragment the antibubble, forcing it to release it's therapeutic content. Releasing the chemotherapeutics at the targeted cancerous site specifically would drastically reduce the systematic damage that is currently endured as a result of the systemic delivery of these toxic chemicals.

References

[1] S. Kotopoulis, K. Johansen, O. H. Gilja, A. T. Poortinga, and M. Postema, "Acoustically active antibubbles," *Acta Physica Polonica A*, vol. 127, no. 2, pp. 99–102, 2015.

[2] M. Postema, A. Novell, C. Sennoga, A. T. Poortinga, and A. Bouakaz, "Harmonic response from microscopic antibubbles," *Applied Acoustics*, vol. 137, no. 1, pp. 148–150, 2018.

[3] M. Postema and O. H. Gilja, "Contrast-enhanced and targeted ultrasound," *World Journal of Gastroenterology*, vol. 17, no. 1, pp. 28–41, 2011.

[4] D. M. Rubin, N. Anderton, C. Smalberger, J. Polliack, M. Nathan, and M. Postema, "On the behaviour of living cells under the influence of ultrasound," *Fluids*, vol. 3, no. 82, pp. 1–19, 2018.

[5] M. Postema, P. Marmottant, C. T. Lancée, S. Hilgenfeldt, and N. de Jong, "Ultrasound-induced microbubble coalescence," *Ultrasound in Medicine and Biology*, vol. 30, no. 10, pp. 1337–1344, 2004.

[6] M. Postema and G. Schmitz, "Bubble dynamics involved in ultrasonic imaging," *Expert Review of Molecular Diagnostics*, vol. 6, no. 3, pp. 493–502, 2006.

[7] S. Fernandes, F. Forsberg, S. C. Gilmore, S. V. Shevchuk, A. Kerschen, T. O. Matsunaga, and R. Zutshi, "Adherence of platelet and fibrin targeted ultrasound contrast bubbles to human blood clots in vitro," in *Proceedings of the IEEE Ultrasonics Symposium*, 2008, pp. 349–352.

[8] M. Postema, F. J. ten Cate, G. Schmitz, N. de Jong, and A. van Wamel, "Generation of a droplet inside a microbubble with the aid of an ultrasound contrast agent: first result," *Letters in Drug Design and Discovery*, vol. 4, no. 1, pp. 74–77, 2007.

[9] M. Postema and G. Schmitz, "Ultrasonic bubbles in medicine: influence of the shell," *Ultrasonics Sonochemistry*, vol. 14, no. 4, pp. 438–444, 2007.

[10] P. Heppner and J. R. Lindner, "Contrast ultrasound assessment of angiogenesis by perfusion and molecular imaging," *Expert Review of Molecular Diagnostics*, vol. 5, no. 3, pp. 447–455, 2005.

[11] N. G. Lee, J. L. Berry, T. C. Lee, A. T. Wang, S. Honowitz, A. L. Murphree, N. Varshney, D. R. Hinton, and A. A. Fawzi, "Sonoporation enhances chemotherapeutic efficacy in retinoblastoma cells in vitro," *Investigative Ophthalmology and Visual Science*, vol. 52, no. 6, pp. 3868–3873, 2011.

[12] A. Delalande, M. Postema, N. Mignet, P. Midoux, and C. Pichon, "Ultrasound and microbubble-assisted gene delivery: recent advances and ongoing challenges," *Therapeutic Delivery*, vol. 3, no. 10, pp. 1199–1215, 2012.

[13] K. Keyhani, H. R. Guzmán, A. Parsons, T. N. Lewis, and M. R. Prausnitz, "Intracellular drug delivery using low-frequency ultrasound: quantification of molecular uptake and cell viability," *Pharmaceutical Research*, vol. 18, no. 11, pp. 1514–1520, 2001.

[14] M. Postema and O. H. Gilja, "Ultrasound-directed drug delivery," *Current Pharmaceutical Biotechnology*, vol. 8, no. 6, pp. 355–361, 2007.

[15] S. Kotopoulis, G. Dimcevski, O. H. Gilja, D. Hoem, and M. Postema, "Treatment of human pancreatic cancer using combined ultrasound, microbubbles, and gemcitabine: a clinical case study," *Medical Physics*, vol. 40, no. 7, p. 072902, 2013.

[16] J. S. Allen, D. J. May, and K. W. Ferrara, "Dynamics of therapeutic ultrasound contrast agents," *Ultrasound in Medicine and Biology*, vol. 28, no. 6, pp. 805–816, 2002.

[17] M. J. Shortencarier, P. A. Dayton, S. H. Bloch, P. A. Schumann, T. O. Matsunaga, and K. W. Ferrara, "A method for radiation-force localized drug delivery using gas-filled lipospheres," *IEEE Transactions on Ultrasonics, Ferroelectrics, and Frequency Control*, vol. 51, no. 7, pp. 822–831, 2004.

[18] S. Dorbolo, H. Caps, and N. Vandewalle, "Fluid instabilities in the birth and death of antibubbles," *New Journal of Physics*, vol. 5, no. 1, p. 161, 2003.

[19] P. G. Kim and H. A. Stone, "Dynamics of the formation of antibubbles," *European Physics Letters*, vol. 83, p. 54001, 2008.

[20] B. Scheid, S. Dorbolo, L. R. Arriaga, and E. Rio, "Antibubbles dynamics: the drainage of an air film with incompressible interfaces," *Physical Review Letters*, vol. 109, no. 26, p. 264502, 2012.

[21] N. Vandewalle, D. Terwagne, T. Gilet, H. Caps, and S. Dorbolo, "Antibubbles, liquid onions and bouncing droplets," *Colloids and Surfaces A: Physicochemical and Engineering Aspects*, vol. 344, no. 1-3, pp. 42–47, 2009.

[22] P. G. Kim and J. Vogel, "Antibubbles: factors that affect their stability," *Colloids and Surfaces A: Physicochemical and Engineering Aspects*, vol. 289, no. 1-3, pp. 237–244, 2006.

[23] A. T. Poortinga, "Long-lived antibubbles: stable antibubbles through pickering stabilization," *Langmuir*, vol. 27, no. 6, pp. 2138–2141, 2011.

[24] K. Johansen and M. Postema, "Lagrangian formalism for computing oscillations of spherically symmetric encapsulated acoustic antibubbles," *Hydroacoustics*, vol. 19, pp. 197–208, 2016.

[25] M. Postema, S. Kotopoulis, and K. Jenerka, *EFSUMB Course Book on Ultrasound*, 2012, ch. Basic Physical Principles of Medical Ultrasound, pp. 9–26.

[26] M. Postema, *Fundamentals of Medical Ultrasonics*, 2014, pp. 177–201.

[27] O. Silberrad, "Propeller erosion," *Engineering*, pp. 33–35, 1912.

[28] C. E. Brennen, *Cavitation and Bubble Dynamics*. New York: Oxford University, 1995.

[29] F. R. Young, *Cavitation*. New York: McGraw-Hill, 1989.

[30] I. Rosenthal, J. Z. Sostaric, and P. Riesz, "Sonodynamic therapy: a review of the synergistic effects of drugs and ultrasound," *Ultrasonics Sonochemistry*, vol. 11, no. 6, pp. 349–363, 2004.

[31] E. L. Carstensen, P. Kelly, C. C. Church, A. A. Brayman, S. Z. Child, C. H. Raeman, and L. Schery, "Lysis of erythrocytes by exposure to CW ultrasound," *Ultrasound in Medicine and Biology*, vol. 19, no. 2, pp. 147–165, 1993.

[32] D. Dalecki, "Mechanical bioeffects of ultrasound," *Annual Review of Biomedical Engineering*, vol. 6, pp. 229–248, 2004.

[33] R. E. Apfel and C. K. Holland, "Gauging the likelihood of cavitation from short-pulse, low-duty cycle diagnostic ultrasound," *Ultrasound in Medicine and Biology.*, vol. 17, no. 2, pp. 179–185, 1991.

[34] The Safety Group of the British Medical Ultrasound Society, "Guidelines for the safe use of diagnostic ultrasound equipment," *Ultrasound*, vol. 18, no. 2, pp. 52–59, 2010.

[35] T. Dehoux, M. Abi Ghanem, O. F. Zouani, J.-M. Rampnoux, Y. Guillet, S. Dilhaire, M.-C. Durrieu, and B. Audoin, "All-optical broadband ultrasonography of single cells," *Scientific Reports*, vol. 5, pp. 86 501–86 505, 2015.

[36] C. Blase and J. Bereiter-Hahn, *Ultrasonic Characterization of Biological Cells.* Boca Raton: CRC Press, 2016, pp. 689–722.

[37] P. Weiss, "The rise of antibubbles: odd, soggy bubbles finally get some respect," *Science News*, vol. 165, no. 20, pp. 311–312, 2004.

[38] A. T. Poortinga, "Micron-sized antibubbles with tunable stability," *Colloids and Surfaces A: Physicochemical and Engineering Aspects*, vol. 419, no. 1, pp. 15–20, 2013.

[39] N. Kudo, R. Uzbekov, R. Matsumoto, R. Shimizu, C. Carlson, N. Anderton, A. Deroubaix, C. Penny, A. T. Poortinga, D. M. Rubin, A. Bouakaz, and M. Postema, "Oscillating endoskeletal antibubbles," in *Proceedings of the 40th Ultrasonics Electronics Symposium*, 2019.

[40] N. Mazzawi, "Bubble-like response of living blood cells in an ultrasound field," MSc, Technion – Israel Institute of Technology, 2013.

[41] T. G. Leighton, *The Acoustic Bubble.* London: Academic Press, 1994.

[42] K. Johansen, S. Kotopoulis, and M. Postema, "Ultrasonically driven antibubbles encapsulated by Newtonian fluids for active leakage detection," in *Proceedings of the International MultiConference of Engineers and Computer Scientists*, vol. 2, 2015, pp. 1–5.

[43] A. A. Doinikov and A. Bouakaz, "Review of shell models for contrast agent microbubbles," *IEEE Transactions on Ultrasonics, Ferroelectrics, and Frequency Control*, vol. 58, no. 5, pp. 981–993, 2011.

[44] M. Postema, A. Bouakaz, C. T. Chin, and N. de Jong, "Simulations and measurements of optical images of insonified ultrasound contrast microbubbles," *IEEE Transactions on Ultrasonics, Ferroelectrics, and Frequency Control*, vol. 50, no. 5, pp. 523–536, 2003.

[45] S. Kotopoulis and M. Postema, "Microfoam formation in a capillary," *Ultrasonics*, vol. 50, no. 2, pp. 260–268, 2010.

[46] L. D. Landau and E. M. K. Lifshitz, *Fluid Mechanics 2nd edition.* Oxford: Butterworth-Heinemann, 1987.

[47] N. Kudo, R. Uzbekov, R. Matsumoto, R. Shimizu, C. S. Carlson, N. Anderton, A. Deroubaix, C. Penny, A. T. Poortinga, D. M. Rubin, A. Bouakaz, and M. Postema, "Asymmetric oscillation of endoskeletal antibubbles," *Japanese Journal of Applied Physics*, 2019 (submitted).

[48] T. L. Szabo, *Diagnostic ultrasound imaging: inside out.* London: Academic Press, 2004.

[49] R. S. C. Cobbold, *Foundations of biomedical ultrasound.* Oxford: Oxford University Press, 2006.

[50] K. K. Shung, "High frequency ultrasonic imaging," *Journal of Medical Ultrasound*, vol. 17, no. 1, pp. 25–30, 2009.

[51] F. Wu, Z.-B. Wang, H. Zhu, W.-Z. Chen, J.-Z. Zou, J. Bai, K.-Q. Li, C.-B. Jin, F.-L. Xie, and H.-B. Su, "Feasibility of US-guided high-intensity focused ultrasound treatment in patients with advanced pancreatic cancer: initial experience," *Radiology*, vol. 236, no. 3, pp. 1034–1040, 2005.

[52] M. H. Yu, J. Y. Lee, H. R. Kim, B. R. Kim, E.-J. Park, H. S. Kim, J. K. Han, and B. I. Choi, "Therapeutic effects of microbubbles added to combined high-intensity focused ultrasound and chemotherapy in a pancreatic cancer xenograft model," *Korean Journal of Radiology*, vol. 17, no. 5, pp. 779–788, 2016.

[53] N. Kudo, "High-speed in situ observation system for sonoporation of cells with size- and position-controlled microbubbles," *IEEE Transactions on Ultrasonics, Ferroelectrics, and Frequency Control*, vol. 64, no. 1, pp. 273–280, 2016.

[54] N. Otsu, "A threshold selection method from gray-level histograms," *IEEE Transactions on Systems, Man, and Cybernetics*, vol. 9, no. 1, pp. 62–66, 1979.